7. SITE 1053[1]

Shipboard Scientific Party[2]

HOLE 1053A

Position: 29°59.5385′N, 76°31.4135′W

Date occupied: 2030 hr, 6 February 1997

Spud hole: 0115 hr, 7 February 1997

Date departed: 1820 hr, 7 February 1997

Time on hole: 21.83 hr (21 hr, 50 min)

Seafloor (drill pipe measurement from rig floor, mbrf): 1641.0

Distance between rig floor and sea level (m): 11.5

Water depth (drill pipe measurement from sea level, m): 1629.5

Total depth (drill pipe measurement from rig floor, mbrf): 1825.0

Penetration (m): 183.2

Number of cores (including cores having no recovery): 20

Total core recovered (m): 189.5

Core recovery (%): 103.4

Oldest sediment cored:
Depth (mbsf): 183.2
Lithology: nannofossil chalk
Age: middle Eocene

HOLE 1053B

Position: 29°59.5391′N, 76°31.4141′W

Date occupied: 1820 hr, 7 February 1997

Spud hole: 1900 hr, 7 February 1997

Date departed: 1800 hr, 8 February 1997

Time on hole: 23.67 hr (23 hr, 40 min)

Seafloor (drill pipe measurement from rig floor, mbrf): 1641.8

Distance between rig floor and sea level (m): 11.5

Water depth (drill pipe measurement from sea level, m): 1630.3

Total depth (drill pipe measurement from rig floor, mbrf): 1824.2

Penetration (m): 182.4

Number of cores (including cores having no recovery): 20

Total core recovered (m): 170.11

Core recovery (%): 93.3

Oldest sediment cored:
Depth (mbsf): 182.4
Lithology: nannofossil chalk
Age: middle Eocene

Principal results: Site 1053 is located at the top of an escarpment cut into the upper part of the Blake Nose. The location of Site 1053 was chosen to recover middle Eocene to upper Eocene deposits and to extend the depth transect into water depths (~1630 meters below sea level [mbsl]) equivalent to the depth of modern intermediate waters. Multichannel seismic (MCS) profile Line TD-5 suggests that the middle Eocene interval is about as expanded at Site 1053 as it is at Site 1051. Reflectors in the MCS line indicate that a substantial thickness of upper Eocene and younger sediments is present at Site 1053 that has not been found at deeper sites. The upper Eocene section is expected to contain a high-temporal-resolution record of ocean structure, magnetic reversals, and biological evolution, particularly during times of rapid climate change such as the late Eocene–Oligocene onset of glaciation and the early to middle Eocene cooling. The lithologic cycles will provide a high-quality cyclostratigraphy to enhance both the magnetochronology and biochronology and to improve correlation among sites along the depth transect. The primary reason for drilling this site was to extend the depth transect up the slope of the Blake Nose for studies of Eocene deeper water structure. An additional goal was to recover sediments belonging to the upper Eocene that could be used to describe the timing of the onset of Antarctic glaciation and the upper Eocene tektite strewn field.

Coring at Site 1053 recovered an exceptionally thick upper Eocene section consisting mainly of siliceous nannofossil ooze. This thick section may reflect periods of increased productivity in the surface waters or enhanced preservation on the seafloor.

The top of the cored interval is a 5- to 37-cm-thick layer with manganese nodules and a drilling slurry of clayey foraminifer ooze that is rich in phosphatic debris, including fish scales and vertebrae. Below this is ~12.5 m of pale yellow upper Eocene siliceous nannofossil ooze with varying amounts of foraminifers and clay. As at Sites 1050, 1051, and 1052, there is a sharp color change from pale yellow to light greenish gray at Site 1053. This sharp color change is time-transgressive across the four sites, and there is no discernible compositional difference in the sediment across this boundary. The green siliceous nannofossil ooze is ~126 m thick in Hole 1053A and ~114 m thick in Hole 1053B. Several ash layers are present including a distinctive 8-cm-thick, highly altered, ash-, clay-, and diatom-rich layer. Although at least 20 species of diatoms are present in this layer, diatoms are not abundant or diverse elsewhere at Site 1053. The preservation of diatoms in this layer may have been enhanced as a result of silica leaching during ash alteration. The lowermost 50 m of cored section consists of middle Eocene greenish gray chalk with varying amounts of nannofossils, siliceous microfossils, and clay. Drilling disturbance has resulted in slight to heavy biscuiting in the core.

Light–dark color alternations within the greenish sediment are common, with the darker intervals more clay rich. Correlating the two holes, however, using magnetic susceptibility and gamma-ray attenuation porosity evaluator (GRAPE) density data from the multisensor track (MST) track and the Minolta color spectrophotometer proved to be difficult, as the signals were noisy mainly because of significant bioturbation. Nevertheless, the shipboard composite section shows that a complete record was most likely recovered.

Shipboard paleomagnetic results are not straightforward and were partially improved post cruise by analyzing discrete samples. The holes span Chrons C13r to C17r, with a possible condensation near the middle to late Eocene boundary (Chron C17n). A detailed biostratigraphy was obtained by the integration of nannofossil, planktonic foraminifer, and radiolarian

[1]Norris, R.D., Kroon, D., Klaus, A., et al., 1998. *Proc. ODP, Init. Repts.,* 171B: College Station, TX (Ocean Drilling Program).

[2]Shipboard Scientific Party is given in the list preceding the Table of Contents.

datum levels. The radiolarians, in particular, appear to be useful at this site. We expect to find evidence for upper Eocene impacts near two well-defined extinction levels of radiolarians in the upper Eocene. The extinction levels were found, but tektites are not visible in the sediment, probably because of extensive bioturbation. It is hoped that shore-based research will detect the tektites and other evidence for impact debris. Detailed biochronologic control and excellent preservation of the calcareous microfossils make this site suitable for meeting our paleoceanographic objectives.

BACKGROUND AND OBJECTIVES

Background

Site 1053 is located at the top of an escarpment cut into the upper part of the Blake Nose. The middle Eocene section at Site 1053 is nearly as expanded as that at Site 1051 and, compared with any sections exposed downdip, preserves younger sediments from the upper Eocene sequence. The location of Site 1053 was chosen to recover upper to middle Eocene deposits and to extend the Leg 171B depth transect into water depths equivalent to the those of modern intermediate waters. The present depth of 1630 mbsl is ~350 m shallower at this site than at Site 1051 and about 670 m shallower than at Site 1050. This depth transect will allow studies of the vertical structure of the Eocene oceans.

Objectives

MCS profile Line TD-5 (see Fig. 3, "Introduction" chapter, backpocket foldout, this volume) suggests that the middle Eocene interval is about as expanded at Site 1053 as it is at Site 1051. Reflectors in the MCS line indicate that the substantial thickness of upper Eocene and younger sediments present at Site 1053 has not been found at deeper sites. The upper Eocene and younger section is expected to contain a high-temporal-resolution record of ocean structure magnetic reversals and biological evolution, particularly during times of rapid climate change, such as the Eocene–Oligocene onset of glaciation and the early to middle Eocene cooling. The primary reason for drilling this site was to extend the depth transect up the slope of the Blake Nose for studies of Eocene deep-water structure. An additional goal was to recover sediments belonging to the upper Eocene and, possibly, the Eocene/Oligocene boundary that could be used to describe the timing of the onset of Antarctic glaciation and debris from the upper Eocene tektite strewn field.

We believed that climate-controlled color and lithologic cycles would be pronounced at Site 1053 because of its more landward position and possibly higher clay content relative to the deeper water sites. The lithologic cycles should provide a high-quality cyclostratigraphy that could enhance both the magnetochronology and biochronology as well as improve correlation among sites along the depth transect.

OPERATIONS

Hole 1053A

After the 5-nmi transit from Site 1052, we deployed a beacon at the Global Positioning System (GPS) coordinates for Site 1053 (proposed site BN-4Alt) at 2030 hr on 6 February 1997. By midnight, the driller was attempting to spud Hole 1053A with the extended core barrel (XCB). The driller gently lowered the bit to determine the seafloor depth and observed a reduction in drill-string weight at 1622 meters below rig floor (mbrf). This was close to the corrected precision depth recorder (PDR) measurement of 1622.4 mbrf, and he assumed that this was the seafloor depth. The bit was rotated and advanced with the XCB for 9.6 m without any discernable weight taken by the formation (reduction in drill-string weight). When we retrieved the core barrel, it was empty. We then attempted an advanced hydraulic piston corer (APC) core over the next 9.6-m interval; it, too, came up empty. On our third attempt at a mudline core, APC Core 171B-1053A-1H (Table 1) recovered a nearly full barrel (9.42 m), which implied a mudline depth of 1641.0 mbrf. This is 18.6 m deeper than the observed PDR water depth.

APC Cores 1H through 15H were taken from 0 to 139.0 mbsf. APC Cores 3H through 15H were oriented using the tensor tool. Core 15H did not achieve a full stroke, so we switched to XCB coring. XCB Cores 16X through 20X were taken to 183.2 mbsf, where coring was terminated. The bit was pulled out of the hole and cleared the seafloor at 1820 hr on 7 February.

Table 1. Site 1053 coring summary.

Core, interval (cm)	Date (February 1997)	Time (UTC)	Depth (mbsf)	Length cored (m)	Length recovered (m)	Recovery (%)
171B-1053A-						
1H	7	0140	0.00-9.50	9.5	9.81	103.30
2H	7	0230	9.50-19.00	9.5	10.10	106.30
3H	7	0335	19.00-28.50	9.5	9.80	103.20
4H	7	0415	28.50-38.00	9.5	9.81	103.30
5H	7	0500	38.00-47.50	9.5	9.80	103.20
6H	7	0545	47.50-57.00	9.5	9.83	103.50
7H	7	0620	57.00-66.50	9.5	9.85	103.70
8H	7	0705	66.50-76.00	9.5	9.88	104.00
9H	7	0740	76.00-85.50	9.5	9.73	102.40
10H	7	0815	85.50-95.00	9.5	9.35	98.40
11H	7	0850	95.00-104.50	9.5	9.94	104.60
12H	7	0940	104.50-114.00	9.5	10.10	106.30
13H	7	1020	114.00-123.50	9.5	9.82	103.40
14H	7	1100	123.50-133.00	9.5	9.98	105.10
15H	7	1155	133.00-139.00	6.0	6.05	100.80
16X	7	1330	139.00-144.70	5.7	8.42	147.70
17X	7	1435	144.70-154.30	9.6	8.36	87.10
18X	7	1545	154.30-163.90	9.6	9.75	101.60
19X	7	1645	163.90-173.50	9.6	9.29	96.80
20X	7	1745	173.50-183.20	9.7	9.83	101.30
Coring totals:				183.2	189.50	103.44
171B-1053B-						
1H	7	1920	0.00-3.90	3.9	3.89	99.70
2H	7	1955	3.90-13.40	9.5	9.96	104.80
3H	7	2040	13.40-22.90	9.5	9.88	104.00
4H	7	2115	22.90-32.40	9.5	9.83	103.50
5H	7	2140	32.40-41.90	9.5	9.88	104.00
6H	7	2225	41.90-51.40	9.5	10.05	105.80
7H	7	2250	51.40-60.90	9.5	9.78	102.90
8H	7	2330	60.90-70.40	9.5	9.70	102.10
9H	8	0010	70.40-79.90	9.5	10.02	105.50
10H	8	0050	79.90-89.40	9.5	7.76	81.70
11H	8	0115	89.40-98.90	9.5	9.97	104.90
12H	8	0215	98.90-108.40	9.5	8.98	94.50
13H	8	0300	108.40-117.90	9.5	9.41	99.10
14H	8	0340	117.90-127.40	9.5	9.77	102.80
15X	8	0520	127.40-134.20	6.8	7.82	115.00
16X	8	0655	134.20-143.90	9.7	9.68	99.80
17X	8	0800	143.90-153.50	9.6	7.09	73.90
18X	8	0905	153.50-163.10	9.6	1.52	15.80
19X	8	1025	163.10-172.70	9.6	5.70	59.40
20X	8	1135	172.70-182.40	9.7	9.42	97.10
Coring totals:				182.4	170.11	93.26

Note: An expanded version of this coring summary table that includes lengths and depths of sections and comments on sampling is included on CD-ROM (back pocket, this volume).

Hole 1053B

Without offsetting the vessel, we spudded Hole 1053B with the APC at 1900 hr on 7 February. The mudline depth calculated from the recovery of the first APC core was 1641.8 mbrf. APC Cores 171B-1053B-1H through 14H were taken from 0 to 127.4 mbsf, after which we switched to XCB coring. Adara heat-flow measurements were obtained at 22.9, 51.4, and 79.9 mbsf (Cores 3H, 6H, and 9H, respectively). XCB Cores 15X through 20X were taken to 182.4

Table 2. Summary of lithologic units drilled at Site 1053.

Lithologic subunit	Hole 1053A	Hole 1053B	Age	Lithology
IA	Interval 1H-1, 0-5 cm	Interval 1H-1, 0-37 cm 0-0.05 mbsf	Pleistocene? to late Eocene 0-0.37 mbsf	Mn oxide nodules; clayey ooze with foraminifers and fish scales
IB	Interval 1H-1, 5 cm, to 2H-3, 69 cm	Interval 1H-1, 37 cm, to 2H-6, 150 cm 0.05-13.19 mbsf	late Eocene 0.37-12.90 mbsf	Nannofossil ooze with siliceous microfossils to siliceous nannofossil ooze
IC	Interval 2H-3, 69 cm, to 15H-CC, 12 cm	Interval 2H-7, 0 cm, to 14H-CC 13.19-139.0 mbsf	late Eocene 12.90-127.4 mbsf	Nannofossil ooze to siliceous nannofossil ooze
ID	Interval 16X-1, 0 cm, to 20X-CC	Interval 15X-1, 0 cm, to 20X-CC 139.0-183.2 mbsf	late to middle Eocene 127.4-182.4 mbsf	Siliceous nannofossil chalk

mbsf. The bit was pulled out of the hole and cleared the seafloor at 1220 hr. We retrieved the drill pipe and spent an extra 3 hr for the routine, end-of-leg bottom-hole assembly (BHA) inspection. At 1800 hr on 8 February, the drilling equipment was secured, and we began the transit back to Site 1050 to core Hole 1050C.

LITHOSTRATIGRAPHY

Description of Lithologic Units

Holes 1053A and 1053B were selected to complete the Eocene depth transect across the Blake Nose. Drilling at Site 1053 recovered a much thicker upper Eocene section than that recovered at the previous sites. We recognized one lithologic unit at Site 1053; we subdivided this unit into four subunits based on variations in color and composition (Table 2; Fig. 1). Composition was determined from smear slides (see Section 5 on CD-ROM, back pocket, this volume). Lateral equivalents of all subunits were recovered at each of the previous sites. The boundaries between subunits were defined using the same criteria used at Sites 1051 and 1052.

Unit I

Description: Manganese oxide nodules, clayey ooze with foraminifers, nannofossil ooze to siliceous nannofossil ooze, and siliceous nannofossil chalk
Intervals: 171B-1053A-1H-1, 0 cm, through 20X-CC; 171B-1053B-1H-1, 0 cm, through 1053B-20X-CC
Depth: 0–183.2 mbsf, Hole 1053A; 0–182.4 mbsf, Hole 1053B
Thickness: 183.2 m, Hole 1053A; 182.4 m, Hole 1053B
Age: Pleistocene to middle Eocene

Lithologic Unit I is divided into four subunits. The upper Subunit IA is a 5- to 37-cm-thick layer with Mn nodules and a drilling slurry of clayey foraminifer ooze that is rich in phosphatic debris, including fish scales and vertebrae. Below this, Subunit IB is ~12.5 m thick and is composed of pale yellow upper Eocene siliceous nannofossil ooze with varying amounts of foraminifers and clay (see Section 4, this volume). As at Sites 1050, 1051, and 1052, there is a sharp color change from pale yellow to light greenish gray, which, at Site 1053, marks the top of Subunit IC (Sections 171B-1053A-2H-3, 69 cm, and 171B-1053B-2H-7, 0 cm). This sharp color change is time-transgressive across the four sites, and there is no discernible compositional difference in the sediment across this boundary. Results from X-ray-fluorescence (XRF) analysis of yellow and green samples from Hole 1051A reveals no significant difference in iron, manganese, titanium, or trace-element levels. Nor is there any difference in the interstitial-water chemistry or the mineral composition, as determined by XRD. We suspect the sharp color change is caused by a slight difference in the redox potential and, thus, by iron and/or manganese oxidation states between the two intervals.

Subunit IC is ~126 m thick in Hole 1053A and ~114 m thick in Hole 1053B. The last occurrence (LO) of ooze constitutes the upper boundary of Subunit ID. This ~50-m-thick middle to upper Eocene subunit consists of greenish gray chalk with varying amounts of nannofossils, siliceous microfossils, and clay. Ash layers identified in Unit I are summarized in Table 3.

Subunit IA

Description: Manganese oxide nodules and foraminifer ooze
Intervals: 171B-1053A-1H-1, 0 cm, to 1H-1, 5 cm; 171B-1053B-1H-1, 0 cm, to 1H-1, 37 cm
Depth: 0–0.05 mbsf, Hole 1053A; 0–0.37 mbsf, Hole 1053B
Thickness: 0.05 m, Hole 1053A; 0.37 m, Hole 1053B
Age: Pleistocene to late Eocene

A drilling slurry of pale brown (10YR 6/3) foraminifer ooze with manganese nodules (as much as 0.5 cm) was recovered in the upper 5 cm of Core 171B-1053A-1H. This Mn-rich interval most likely corresponds to the Mn oxide layer recovered at the top of Sites 1049, 1050, 1051, and 1052, where it was also designated as lithologic Subunit IA. In Hole 1053B, Subunit IA comprises nodules of Mn oxide and phosphate foraminifer ooze, with Pleistocene-aged nannofossils and Mn nodules that are as much as 4 cm in size. The base of Subunit IA is placed at the lithologic change from pale brown foraminifer ooze to pale yellow (2.5Y 8/1) nannofossil ooze. Subunit IA is highly disturbed in Hole 1053A and moderately to highly disturbed in Hole 1053B.

Subunit IB

Description: Nannofossil ooze with siliceous microfossils to siliceous nannofossil ooze
Intervals: 171B-1053A-1H-1, 5 cm, to 2H-3, 69 cm; 171B-1053B-1H-1, 37 cm, to 2H-6, 150 cm
Depth: 0.05–13.19 mbsf, Hole 1053A; 0.37–12.9 mbsf, Hole 1053B
Thickness: 13.1 m, Hole 1053A; 12.5 cm, Hole 1053B
Age: late Eocene

Subunit IB is a middle Eocene nannofossil ooze with siliceous microfossils (diatoms, radiolarians, and sponge spicules) to siliceous nannofossil ooze. The base of lithologic Subunit IB is defined by a sharp change in color from pale yellow (5Y 8/1–8/2) to the light greenish gray (5G 8/1 to 10GY 8/1) of the underlying Subunit IC sediment. In general, bedding is poorly defined, and the sediment is homogeneous. Burrow mottling is slight to moderate. Pyrite flecks are disseminated throughout the subunit.

Subunit IC

Description: Nannofossil ooze to siliceous nannofossil ooze
Intervals: 171B-1053A-2H-3, 69 cm, through 15H-CC, 12 cm; 171B-1053B-2H-7, 0 cm, through 14H-CC
Depth: 13.19–139.0 mbsf, Hole 1053A; 12.9–127.4 mbsf, Hole 1053B
Thickness: 125.81 m, Hole 1053A; 114.5 m, Hole 1053B
Age: late Eocene

The top of Subunit IC is defined by a sharp color change from the overlying pale yellow (5Y 8/1–8/2) Subunit IB sediment to the varying shades of greenish gray (5G 8/1 to 10GY 8/1) sediment of Sub-

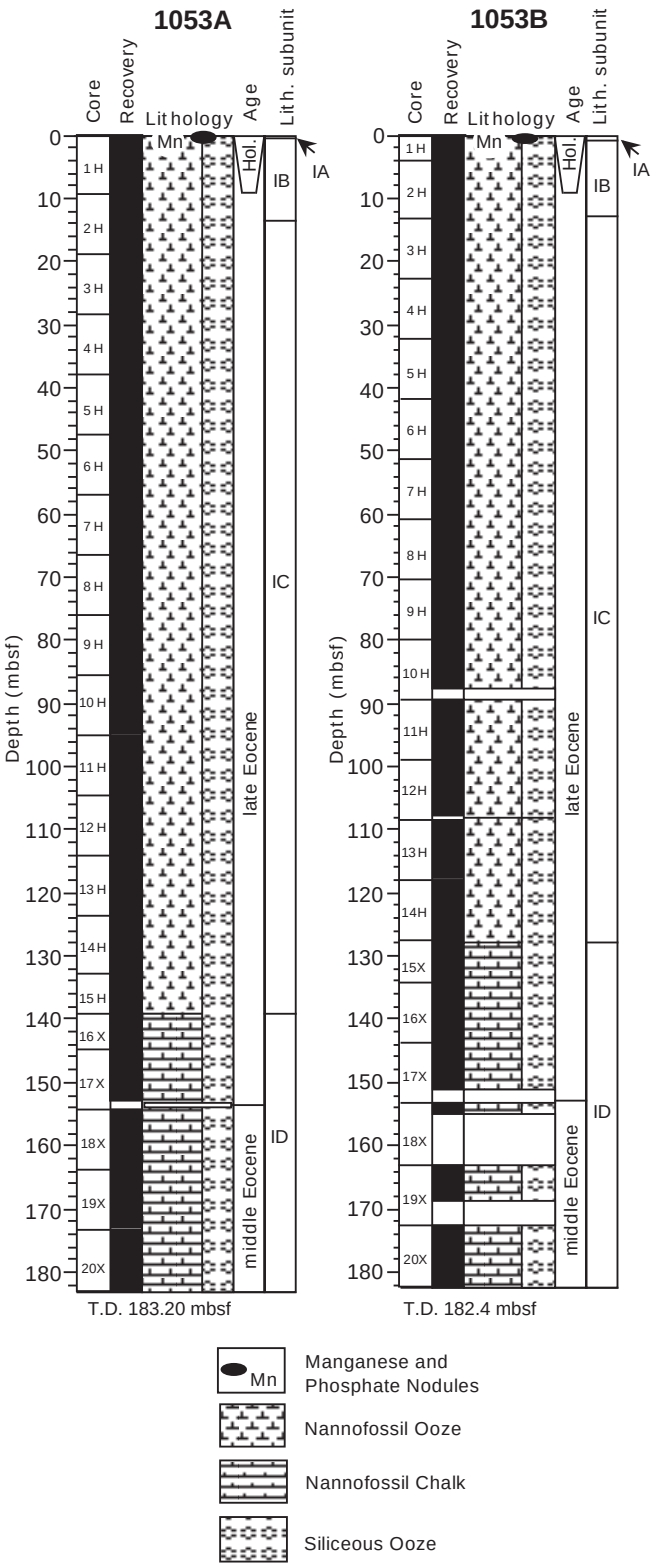

Figure 1. Summary of lithology, core recovery, and age for sediment recovered from Holes 1053A and 1053B.

Table 3. Ash layers recovered at Site 1053.

Core, section, interval (cm)	Depth (mbsf)	Comments
171B-1053A-		
1H-2, 99-102	2.52	Vitric ash
171B-1053B-		
1H-2, 120-122	2.65-2.67	Vitric ash
171B-1053A-		
2H-6, 53	17.53	Vitric ash
8H-2, 76-84	68.76-68.84	Altered ash with diatoms
171B-1053B-		
8H-5, 50-57	67.40-67.47	Altered ash with diatoms
171B-1053A-		
9H-3, 5-9	79.05-79.09	Vitric ash
9H-6, 112-122	84.62-84.72	Vitric ash
171B-1053B-		
10H-3, 39-45	83.29-83.35	Vitric ash
171B-1053A-		
10H-5, 134	92.84	Vitric ash
19X-1, 64-66	164.54-164.56	Vitric ash

unit IC. Light–dark color alternations within the greenish sediment are commonly visible, with the darker intervals more clay rich. Subunit IC is upper Eocene nannofossil ooze with siliceous microfossils to siliceous nannofossil ooze. Burrow mottling is moderate to intensive, typically with pale brown burrows that are often enriched in siliceous microfossils. The sediment is slightly to moderately bioturbated; burrows include *Chondrites*, *Planolites*, *Zoophycos*, and unidentified burrows. Pyrite is disseminated throughout in the form of flecks, burrow linings, and burrow fills. Some burrows are filled with glauconite-rich sediment. Several ash layers are present in Subunit IC, including a distinctive 8-cm-thick, highly altered, clay- and diatom-rich layer that is readily recognized in Cores 171B-1053A-8H and 171B-1053B-8H (Table 3). At least 20 species of diatoms are present in this layer, whereas diatoms are not abundant or diverse in the remainder of Unit I. Preservation of diatoms in this layer may have been enhanced because of increased silica levels generated during ash alteration. The last downhole occurrence of ooze constitutes the lower boundary of Subunit IC.

Subunit ID

Description: Siliceous nannofossil chalk
Intervals: 171B-1053A-16X-1, 0 cm, through 20X-CC; 171B-1053B-15X-1, 0 cm, through 20X-CC
Depth: 139.0–183.2 mbsf, Hole 1053A; 127.4–182.4 mbsf, Hole 1053B
Thickness: 44.2 m, Hole 1053A; 55.0 m, Hole 1053B
Age: middle to late Eocene

The top of Subunit ID is marked by the change from Subunit IC ooze to the chalk of Subunit ID. This light greenish gray chalk is slightly to intensively bioturbated with *Chondrites*, *Planolites*, *Teichichnus*, *Zoophycos*, and undifferentiated burrows. Pyrite is disseminated throughout in the form of flecks, burrow linings, and burrow fills. Drilling disturbance has resulted in slight to heavy biscuiting in the core.

Discussion

All four subunits of lithologic Unit I were also recovered at previous sites, and their origin is discussed in those site chapters. Site 1053 differs from previous sites in that an exceptionally thick upper Eocene section of siliceous nannofossil ooze was recovered. This thick section may reflect periods of increased productivity in the surface waters or enhanced preservation on the seafloor. The presence of abundant diatoms in an altered ash layer in Subunit IC suggests increased production of biogenic silica associated with ash deposition.

However, with the exception of that interval, siliceous microfossils are not noticeably more abundant at Site 1053 than at previous sites, where the upper Eocene section is more condensed. Alternatively, diatoms may have been preferentially preserved in the ash layer because of silica leaching during alteration.

Seven ash layers are present in the Eocene section of Hole 1053A (Table 3), whereas only three are recognized in Hole 1053B. However, many of these ash layers are only 1–2 cm thick, and others may have been obscured by bioturbation, which is pervasive throughout Subunits IC and ID. Alternatively, the ash layers may have been disturbed by drilling, particularly in the highly biscuited Subunit ID. We note that trace amounts of volcanic glass and biotite were found in smear slides from intervals far from recognizable ash layers. Possible source areas for the ash are discussed in the "Lithology" section of the "Site 1050" chapter (this volume).

Nondeposition or erosion of sediment has persisted from the late Eocene to the present. A Mn oxide sand and nodule layer <5 cm thick is all that represents this interval.

BIOSTRATIGRAPHY

Calcareous Nannofossils

Calcareous nannofossil biostratigraphy was based primarily on examination of core-catcher material, supplemented by other closely spaced samples from Holes 1053A and 1053B. These two holes form a nearly complete composite section that spans the uppermost Eocene –uppermost middle Eocene (Fig. 2). Calcareous nannofossil datums and their depths are listed in Table 4.

The upper 139 m of sediment consists of upper Eocene oozes containing moderately to well-preserved calcareous nannofossil assemblages. The presence of *Discoaster saipanensis* and the absence of *D. barbadiensis* in Core 171B-1053A-1H constrain the age at the top of Hole 1053A to between 34.2 and 34.3 Ma, using the Berggren et al. (1995) time scale. The presence of *Ismolithus recurvus* in the upper 80–90 m of sediment from Holes 1053A and 1053B indicates late Eocene Subzone CP15b. The occurrence of *I. recurvus* is frequent at the top of this section but is sporadic near the bottom of its range, suggesting that a more detailed examination of material taken at more closely spaced intervals may extend this subzone downward in the core.

The lower upper Eocene Subzone CP15a occurs from Core 171B-1053A-9H through Section 171B-1053A-18X-6 and is based on the presence of *Chiasmolithus oamaruensis* and on the absence of *Ismolithus recurvus.* Reworking of the upper middle Eocene marker species, *C. grandis,* into the basal Subzone CP15a, along with sporadic occurrences of *C. oamaruensis,* makes this boundary difficult to ascertain. Sediments throughout the lower upper Eocene consist of calcareous nannofossil oozes containing high concentrations of siliceous biogenic material from the surface to 140 m, where they become predominantly calcareous nannofossil chalks.

The upper middle Eocene extends from Section 171B-1053-18X-CC to the bottom of the hole and consists of calcareous nannofossil chalks with high amounts of siliceous material. Placement within calcareous nannofossil Subzone CP14b is based on the presence of *Chiasmolithus grandis* and on the absence of *C. oamaruensis.* Co-occurrence of *C. grandis* with *Dictyococcites bisectus* suggests placement in the uppermost portion of Subzone CP14b according to the Berggren et al. (1995) time scale. However, *D. bisectus* has been found consistently to occur in strata older than its published range at all Leg 171B sites where it is present. Based on the assumption that the range of *D. bisectus* is greater than previously recorded, correlation between calcareous nannofossil and planktonic foraminifer datums throughout this interval is good (Fig. 2).

Planktonic Foraminifers

The 183-m sequence at Site 1053 ranges from late to middle Eocene (Zones P16–P14) in age. Zonal assignments for Holes 1053A and 1053B are summarized in Figures 2 and 3, and distribution charts are presented in Tables 5 and 6. Only biostratigraphic results from Hole 1053A were used to calculate the sediment accumulation rates, as the datums there were more precisely defined (Table 7).

Foraminifers are well preserved in all samples examined, and they occur in high abundance in the upper part of the recovered sequence and in moderate to low abundances in the middle and lower parts. Intervals of lower abundance are the result of dilution by radiolarians, sponge spicules, and other siliceous microfossils.

Biostratigraphic results for Holes 1053A and 1053B are in good agreement for all the marker species identified. Upper Eocene Zone P16 was recovered in the upper ~60 m of both holes. The base of this zone is identified in Sample 171B-1053A-7H-2, 70–71 cm (59.2 mbsf), and Sample 171B-1053B-7H-CC, 10–11 cm (61.1 mbsf), by the first occurrence (FO) of *Turborotalia cunialensis. Cribrohantkenina inflata* occurs consistently down to its FO in Sample 171B-1053A-7H-4, 70–71 cm (62.2 mbsf). According to Berggren et al. (1995), this datum is correlative with the top of Zone P15. Specimens that are morphologically very similar to *C. inflata,* but lack multiple areal apertures, occur within 10 m of the FO of *C. inflata* (sensu stricto) in both holes.

The base of Zone P15, defined by the FO of *Porticulasphaera semiinvoluta,* is placed at the same level (181.2 mbsf) in Holes 1053A and 1053B (Samples 171B-1053A-20X-6, 24–28 cm, and 171B-1053B-19X-CC, 33–36 cm). Although Berggren et al. (1995) suggest that the extinction of *P. semiinvoluta* is synchronous with the extinction of *Turborotalia pomeroli,* the range of the latter species extends one core above the former. In the upper part of Zone P15 the gradual morphological transition from *T. cocoaensis* to *T. cunialensis* is well represented. The FO of *Hantkenina alabamensis* is in lower Zone P15, which is two cores from the top of Zone P14. The range of this species extends to the top of the cored sequence. The highest occurrence of *Acarinina* is recorded by a small, moderately spired form that has not been described previously. This taxon is consistently present in low abundance from upper Zone P14 to Section 171B-1053A-18X-CC in lower Zone P15.

The coincidence of the LOs of *Morozovella spinulosa* and *Acarinina collactea* in Sample 171B-1053A-19X-CC suggests that there is a hiatus within Core 171B-1053A-19X, as Berggren et al. (1995) record the LO of the latter species to be 0.4 m.y. after that of *M. spinulosa.* Evidence for this hiatus is corroborated by the sediment accumulation rate plot (Fig. 3), which suggests that about 1 m.y. is missing between the LO of the nannofossil species *Chiasmolithus grandis* (37.1 Ma) in Section 171B-1053A-18X-CC and the co-occurring LOs of *M. spinulosa* (38.1 Ma) and *A. collactea* (37.7 Ma) in Section 171B-1053A-19X-CC. The LOs of *Truncorotaloides rohri* and *A. bullbrooki* are also in Section 171B-1053A-19X-CC, adding further support for the presence of a hiatus within Core 171B-1053A-19X. However, because no change in color or lithology has been observed in the core, there is no physical evidence for this hiatus.

The top of Zone P14 was barely penetrated in Holes 1053A and 1053B. Except for the absence of *P. semiinvoluta,* the assemblage from this interval is very similar to the assemblage from lowermost Zone P15.

The LOs of *Acarinina primitiva, A. bullbrooki,* and *Subbotina linaperta* are not used to estimate sediment accumulation rates at Site 1053 because these datums occur much higher than the relative positions suggested by Berggren et al.'s (1995) biostratigraphic scheme. The LO of *S. linaperta* at 19.6 mbsf plots at about 34.6 Ma in Figure

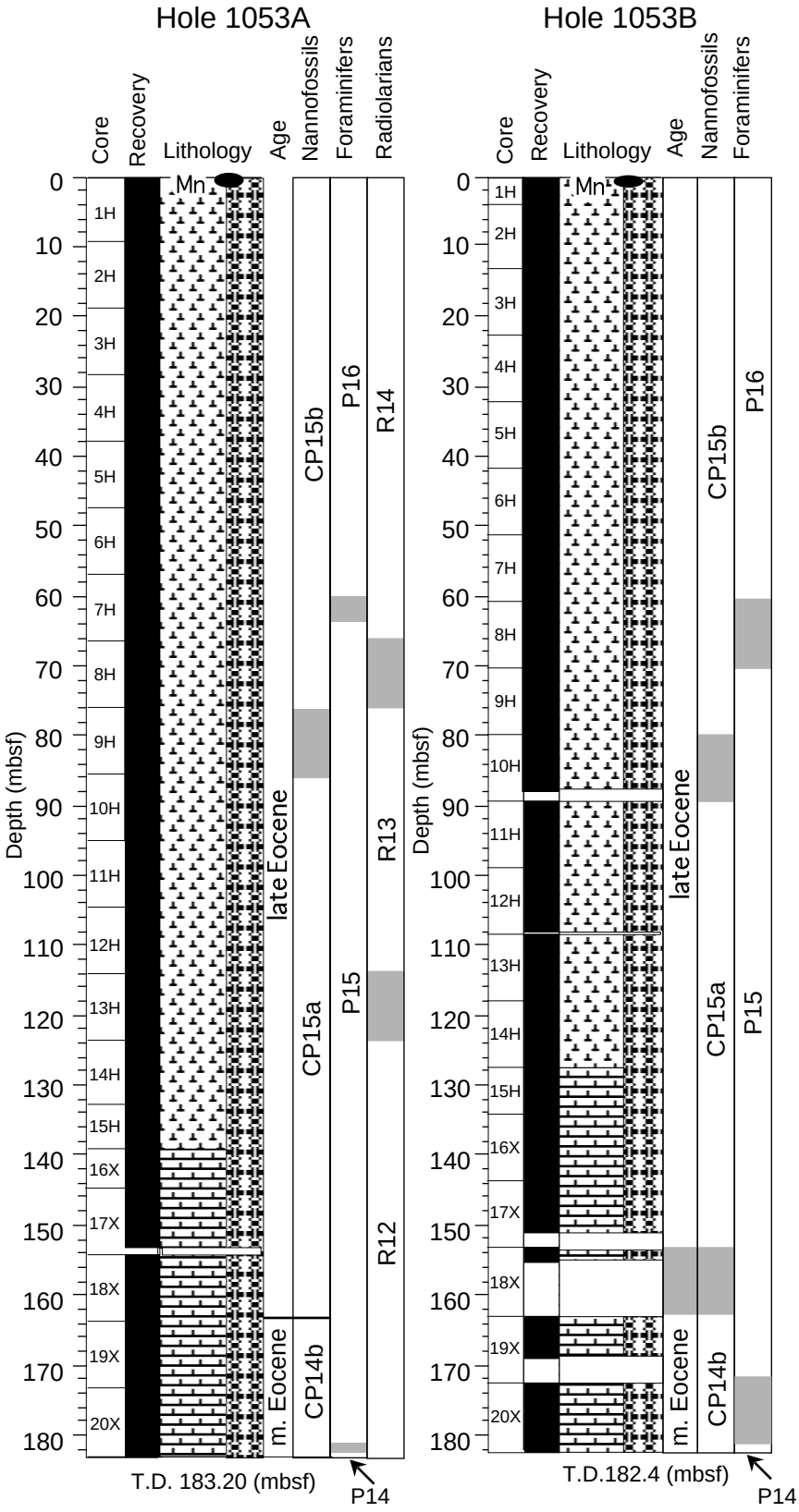

Figure 2. Distribution of biostratigraphic units and ages in Holes 1053A and 1053B. Shaded areas indicate uncertainty caused by sample spacing or poor preservation. Lithologic symbols are the same as in Figure 1.

Table 4. Calcareous nannofossil datums for Site 1053.

Datum	Species	Zone	Age (Ma)	Core, section, interval (cm)	Minimum depth (mbsf)	Maximum depth (mbsf)
				171B-1053A-		
T	*D. barbadiensis*		34.30	2H-1 66-67	9.8	10.2
T	*C. reticulatum*		35.00	3H-CC	27.2	28.8
B	*I. recurvus*	b CP15b	36.00	8H-CC	76.4	85.7
B	*C. oamaruensis*		37.00	18X-6 91-92	162.7	164.0
T	*C. grandis*	t CP14b	37.10	18X-CC	162.7	164.1
				171B-1053B-		
T	*D. barbadiensis*		34.30	2H-CC	3.8	13.8
B	*I. recurvus*	b CP15b	36.00	9H-CC	80.4	87.6
B	*C. oamaruensis*		37.00	17X-CC	151.0	155.0
T	*C. grandis*	t CP14b	37.10	18X-CC	151.0	155.0

Notes: Bases of age and biozonal datums are represented by B and b; tops of age and biozonal datums are represented by T and t.

3, but Berggren et al. (1995) indicate that the extinction of this species was at 37.7 Ma. Similarly, the LOs of *A. primitiva* (~175 mbsf) and *A. bullbrooki* (153 mbsf) plot at 38.2 and 36.8 Ma, respectively, whereas Berggren et al. (1995) record the extinction of *A. primitiva* and *A. bullbrooki* at 39 Ma and 40.5 Ma, respectively. Because there is no evidence for reworking of these species at Site 1053 and because these higher occurrences were also observed at Site 1050, it is likely that Berggren et al.'s (1995) age estimates for these extinction datums will need to be revised.

Benthic Foraminifers

The preservation of benthic foraminifers is good to very good throughout the upper to middle Eocene sediments cored in Hole 1053A, and they occur in relatively high abundances (see Table 8). Site 1053 paleodepths of middle to late Eocene times are estimated to be the upper part of the middle bathyal realm (~500–700 m), based on the presence of several upper bathyal taxa such as *Bolivina byramensis, Hanzawaia ammophila, Planulina ambigua,* and *Uvigerina rippensis;* the patchy occurrence of *Nuttallides truempyi;* and the absence of several lower bathyal species such as *Aragonia* spp., *Gaudryina pyramidata,* and *Quadrimorphina profunda.*

Only a few taxa (*Bulimina* cf. *semicostata, B. macilenta,* and *Buliminella grata spinosa*) were restricted to the lowermost Sample 171B-1053A-20X-CC, 39–41 cm, of middle Eocene age (planktonic foraminifer Zone P14), whereas virtually all of the remaining taxa in this sample (i.e., *Anomalinoides spissiformis, Bulimina trinitatensis, Cibicorbis herricki, Cibicidoides praemundulus, Gyroidinoides girardanus, Nodogenerina* spp., *Nuttallides truempyi, Oridorsalis* spp., and *Pullenia eocaenica*) ranged into the upper Eocene Zone P16.

Out of the 21 taxa originating in the middle to upper Eocene Zone P15, six taxa (*Bulimina tuxpamensis, Cibicidoides grimsdalei, Gavelinella capitata, Gyroidinoides* spp., *Hanzawaia ammophila,* and *Karreriella chapapotensis*) did not range into the upper Eocene Zone P16. Consequently, 15 taxa ranged into Zone P16, including *Bolivina* sp. (slender), *Bulimina alazanensis, C. mexicanus, Globocassidulina punctata, Globocassidulina*? sp. (compressed), *G. subglobosa, Gyroidinoides depressus, Nonion* spp., *Nonionella* spp., *Planulina ambigua,* pleurostomellids, *Pullenia* spp., *Vulvulina spinosa, Uvigerina rippensis,* and *Uvigerina* sp. Finally, seven taxa were restricted to the upper Eocene Zone P16, including *Bolivina byramensis, Bulimina glomarchallengeri, B. impendens, Osangularia mexicana, Plectofrondicularia paucicostata, Tritaxa* spp. and *Vulvulina mexicana.*

Radiolarians

Radiolarians were recovered in all core-catcher samples from Hole 1053A. Samples from Hole 1053B were not taken because of time constraints. The preservation of the radiolarians was generally good in Sections 171B-1053A-1H-CC to 13H-CC and, with the exception of Section 19X-CC, was poor from Cores 171B-1053A-14H through 20X. The poor preservation and dilution of many of these faunas is attributed to test dissolution and high clay sedimentation, respectively. The zonal numbers R12 through R14 (see "Explanatory Notes" chapter, this volume) are used in the biostratigraphic correlation shown in Figure 2. Occurrence, abundance, and preservation of the radiolarian taxa are shown in Table 9.

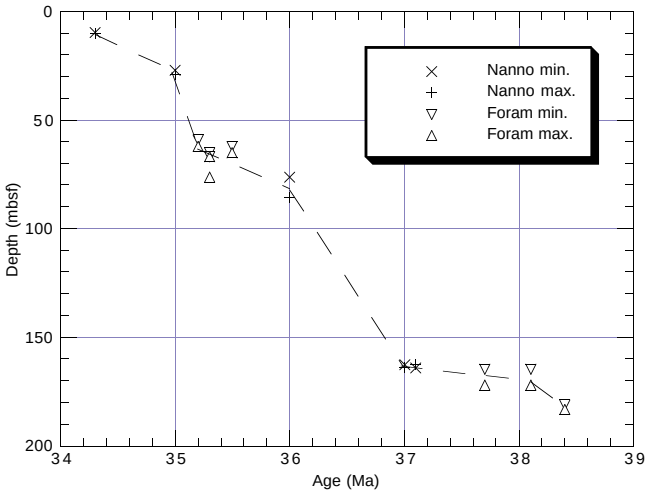

Figure 3. Age-depth relationship at Site 1053, based on calcareous nannofossil and planktonic foraminifer data from Hole 1053A.

The radiolarian faunas recovered represent the three youngest radiolarian zones established for low-latitude Eocene sediments. The youngest faunas, assignable to the *Cryptocarpium ornatum* Zone (Zone R14), were found in Sections 171B-1053A-1H-CC through 7H-CC. The recovery of the Zone R14 faunas, in addition to those assignable to Zones R2 through R13 found at Sites 1050 through 1052, indicates that radiolarians were abundant in the western Atlantic in the Blake Nose area for nearly the entire Eocene.

The boundary between the *Cryptocarpium ornatum* Zone (Zone R14) and the underlying *Calocyclas bandyca* Zone (Zone R13) is defined as the last appearance of *Thyrsocyrtis tetracantha* as well as the LOs of *C. bandyca, C. hispada, Lychnocanoma bellum,* and *Podocyrtis papalis.* This extinction event occurs somewhere between core-catcher samples 171B-1053A-7H-CC and 8H-CC. Sample 171B-1053A-7H-CC contains taxa characteristic of the lower part of the *C. ornatum* Zone, including *Calocyclas turris, Cryptocarpium azyx, Thyrsocyrtis bromia,* and *T. rhizodon.* The extinction of these four taxa occurs somewhere in the interval between Samples 171B-1053A-6H-CC and 7H-CC and marks an impact event reported by Saunders et al. (1984), Sanfilippo et al. (1985), and Clymer et al. (1996).

Samples 171B-1053A-8H-CC through 12H-CC contain faunas assignable to the *Calocyclas bandyca* Zone (Zone R13). The base and top of the zone are defined by the morphotypic first and last appearances of the taxon *C. bandyca.* This species, although rare to moderate in abundance, is distinct in possessing three feet that are subcylindrical in cross section and an inflated thorax. Two other markers, *Dictyoprora armadillo* and *Thyrsocyrtis bromia,* make their first appearances in Sections 171B-1053A-10H-CC and 11H-CC, respectively.

Sections 171B-1053A-13H-CC through 20X-CC contained radiolarians indicative of the upper middle to upper Eocene *Cryptocarpium azyx* Zone (Zone R12). The base of this zone is defined by the first appearance of the species *C. azyx.* The distinct taxon *Calocyclas turris* makes its first appearance within the zone in Section 171B-1053A-18X-CC and is the only radiolarian species reportedly to

Table 5. Distribution chart for planktonic foraminifers from Hole 1053A.

Age	Zone	Core, section, interval (cm)	Depth (mbsf)	Abundance	Preservation	*Acarinina bullbrooki*	*Acarinina primitiva*	*Chiloguembelina cubensis*	*Globigerinatheka index*	*Globigerinatheka mexicana*	*Morozovella spinulosa*	*Subbotina linaperta*	*Subbotiona venezuelana*	*Truncorotaloides rohri*	*Turborotalia cerroazulensis*	*Porticulasphaera semiinvoluta*	*Turborotalia pomeroli*	*Turborotalia possagnoensis*	*Subbotina cryptomphala*	*Turborotalia cocoaensis*	*Acarinina collactea*	*Globigerinatheka rubriformis*	*Subbotina praeturritilina*	*Hantkenina alabamensis*	*Hantkenina liebusi*	*Globorotaloides suteri*	*Pseudohastigerina micra*	*Catapsydrax dissimilis*	*Subbotina eocaena*	*Subbotina hagni*	*Cribrohantkenina inflata*	*Turborotalia cunialensis*
		171B-1053A-																													
late Eocene	P16	1H-CC, 20-23	9.78	C	G				R				F		R					F				R			R		F	F	P	R
late Eocene	P16	2H-CC, 29-32	19.57	F	G							F	F						R	R				R			R		F	F		R
late Eocene	P16	3H-CC, 17-20	28.77	R	G							R	R		P					R				P			R		R			R
late Eocene	P16	4H-CC, 23-25	38.29	A	G			R				F			R									F			R		F	F	P	R
late Eocene	P16	5H-CC, 21-23	47.78	F	G			R				F	F		R									P			R	R	F	F	P	R
late Eocene	P16	6H-CC, 26-28	57.31	F	G			R				F	F		P									R			R	P	F		P	R
late Eocene	P16	7H-2 70-71	59.20	A	VG																						F				P	R
late Eocene	P15	7H-4 70-71	62.20	A	VG				R			F			P												R				R	
late Eocene	P15	7H-6 70-71	65.20	A	VG							F			R					R							R					
middle-late Eocene	P15	7H-CC, 21-23	66.83	F	G			R				F	F		R		P										R	R	F	F		
middle-late Eocene	P15	8H-CC, 25-27	76.36	F	G							F	F		R	P	R		R								R		F	F		
middle-late Eocene	P15	9H-CC, 12-15	85.70	F	G			R	R			F	F		F	F											R		F	F		
middle-late Eocene	P15	10H-CC, 0-4	94.81	A	G			R				A	F		F	R	P										R	F	A	A		
middle-late Eocene	P15	11H-CC, 24-26	104.92	C	G							F	F		R	F	R										R	R	F	F		
middle-late Eocene	P15	12H-CC, 27-29	114.58	C	G			P				F	F		R	F			R					F			R	R	F	F		
middle-late Eocene	P15	13H-CC, 12-15	123.79	C	G			R				F	F		R	F								R			P	R	F	F		
middle-late Eocene	P15	14H-CC, 30-32	133.46	C	G			R		P		R	F		R	F											R	R	F	F		
middle-late Eocene	P15	15H-CC, 11-12	139.04	A	VG							F			R	F	F															
middle-late Eocene	P15	16X-CC, 15-18	147.39	A	VG					F		F			R	F	F										F					
middle-late Eocene	P15	17X-CC, 25-27	153.04	A	VG				R			F				F									P	R						
middle-late Eocene	P15	18X-CC, 27-29	164.03	A	VG				R	F		F			F	F	R							P	P							
middle-late Eocene	P15	19X-1, 73-75	164.65	A	VG				R	F		F			R	R				P		F										
middle-late Eocene	P15	19X-4, 80-83	169.20	A	VG				R	F					R	R	P			P		F										
middle-late Eocene	P15	19X-6, 57-59	171.97	A	VG	R			R	F	P	F		P	R	R	R			P	P	F										
middle-late Eocene	P15	19X-CC, 17-19	173.17	A	VG	F			R	F	R	F		R	R	R	F				P	F	P									
middle Eocene	P15	20X-2, 8.5-11.5	175.09	A	G		P			F		F		R	R	R	R		R	R												
middle Eocene	P15	20X-4, 139.5-142	179.40	A	G	R	P			F	R	F		R		R	R															
middle Eocene	P15	20X-6, 24-28	181.24	A	G	F	R		R		R	F		P		R	F	R														
middle Eocene	P14	20X-CC, 39-41	183.31	A	G	F	R	R	R	F	F	F	R	R	F																	

Notes: Abundance: C = common; F = few; R = rare; A = abundant; P = present. Preservation: G = good; VG = very good.

Table 6. Distribution chart for planktonic foraminifers from Hole 1053B.

Age	Zone	Core, section, interval (cm)	Depth (mbsf)	Abundance	Preservation	*Acarinina bullbrooki*	*Acarinina collactea*	*Acarinina primitiva*	*Globigerinatheka index*	*Globigerinatheka mexicana*	*Morozovella spinulosa*	*Subbotina linaperta*	*Turborotalia cerroazulensis*	*Turborotalia pomeroli*	*Catapsydrax dissimilis*	*Porticulasphaera semiinvoluta*	*Pseudohastigerina micra*	*Truncorotaloides rohri*	*Hantkenina alabamensis*	*Chiloguembelina cubensis*	*Turborotalia cocoaensis*	*Subbotiona venezuelana*	*Cribrohantkenina inflata*	*Turborotalia cunialensis*
		171B-1053B-																						
late Eocene	P16	1H-CC, 12-14	3.87	A	VG				F			F							R		F		R	R
late Eocene	P16	2H-CC, 15-17	13.84	A	VG							F					F		F		F		R	F
late Eocene	P16	3H-CC, 25-27	23.26	A	VG														R		F		R	F
late Eocene	P16	4H-CC, 7-9	32.71	A	VG							F							R		R		F	R
late Eocene	P16	5H-CC, 19-20	42.27	A	VG							F					F		R		F		F	R
late Eocene	P16	6H-CC, 31-33	51.93	A	VG				R			F	F				F		R		F		R	R
late Eocene	P16	7H-CC, 10-11	61.17	C	G							F	F				F		R				R	P
middle-late Eocene	P15	8H-CC, 8-10	70.58	C	G							F	F				R			R	R	R		
middle-late Eocene	P15	9H-CC, 38-42	80.38	C	G							F	F				R				R	R		
middle-late Eocene	P15	10H-CC, 13-17	87.62	C								F	F		R	P	R				R			
middle-late Eocene	P15	11H-CC, 26-28	99.35	C	G							F	F		F		R				R			
middle-late Eocene	P15	12H-CC, 10-12	107.86	C	G							F	F	R	F	P	R		R	R				
middle-late Eocene	P15	13H-CC, 0-2	117.79	C	G							F	F	P	F		R		R					
middle-late Eocene	P15	14H-CC, 27-30	127.64	C	G					P		F	F	R	R	P	R		P					
middle-late Eocene	P15	15X-CC, 40-42	135.2	C	G							F	F	R	R		R		R	R				
middle-late Eocene	P15	16X-CC, 24-27	143.85	F	G							F	F		R		R							
middle-late Eocene	P15	17X-CC, 28-31	150.96	A	G							F	F	P	F	P	R		R					
middle-late Eocene	P15	18X-CC, 15-18	154.99	F	VG							F	R		P	P	R							
middle-late Eocene	P15	19X-CC, 33-36	168.77	A	G	R			P	F	F	F	F		R	P	R	P						
middle Eocene	P14	20X-CC, 35-38	182.09	C	G	R	P	R	R	F	P	F	F	R										

Notes: Abundance: A = abundant; C = common; F = few; R = rare; P = present. Preservation: VG = very good; G = good.

Table 7. Planktonic foraminifer datum list for Hole 1053A.

Datum	Species	Core, section, interval (cm)	Zone	Age (Ma)	Minimum depth (mbsf)	Maximum depth (mbsf)
		171B-1053A-				
B	*T. cunialensis*	7H-2 70-71	b P16	35.20	59.20	62.20
T	*T. pomeroli*	7H-CC, 21-23		35.30	65.20	66.83
T	*P. semiinvoluta*	8H-CC, 25-27		35.30	66.83	76.36
B	*C. inflata*	7H-4, 70-71		35.50	62.20	65.20
T	*A. collactea*	19X-CC, 17-19		37.70	164.65	171.97
T	*M. spinulosa*	19X-CC ,17-19		38.10	164.65	171.97
B	*P. semiinvoluta*	20X-6, 24-28	b P15	38.40	181.24	183.31

Notes: Bases of age and biozonal datums are represented by B and b; tops of age and biozonal datums are represented by T and t.

Table 8. Hole 1053A samples examined for benthic foraminifers.

Core, section, interval (cm)	Age	Zone	Depth (mbsf)	Abundance	Preservation
171B-1053A-					
1H-CC, 20-23	late Eocene	P16	9.78	Common	Good
3H-CC, 17-20	late Eocene	P16	28.77	Abundant	Good
5H-CC, 21-23	late Eocene	P16	47.78	Abundant	Good
7H-CC, 21-23	middle-late Eocene	P15	66.83	Abundant	Good
10H-CC, 0-4	middle-late Eocene	P15	94.81	Abundant	Good
13H-CC, 12-15	middle-late Eocene	P15	123.79	Common	Good
16X-CC, 15-18	middle-late Eocene	P15	147.39	Abundant	Very good
20X-CC, 39-41	middle Eocene	P14	183.31	Common	Good

mark the boundary between the middle and upper Eocene. Inflated forms of *Eusyringium fistuligerum* also are common throughout the zone. The species *Lychnocanoma amphitrite*, although sturdy in test construction, is very rare in the Leg 171B sediments and occurs only in Section 171B-1053A-19X-CC. Also, the important, but fragile, marker species, *Podocyrtis chalara*, makes its last appearance in Section 171B-1053A-18X-CC.

Sediment Accumulation Rates

Ages and sub-bottom depths for calcareous nannofossil and planktonic foraminifer datums used to calculate sediment accumulation rates in Hole 1053A are listed in Tables 4 and 7 and plotted in Figure 2. The 183-m interval cored at this site ranges in age from 34.3 to 38.4 Ma. The sediment accumulation rate for the upper Eocene is extremely high for an open-ocean pelagic setting at 55 m/m.y., reflecting increased biogenic siliceous input. Sedimentation rates for the upper middle Eocene are only slightly lower at 45 m/m.y. (Fig. 3).

A significant change in the rate of sediment accumulation occurred just below the middle to upper Eocene boundary (Fig. 3), between 164 and 173 mbsf. This may be a disconformity with a hiatus spanning ~1 Ma. However, there is no physical manifestation of such a disconformity in the sediments. Alternatively, the rate of sediment accumulation may have slowed to <10 m/m.y. between ~37 and 38.2 Ma. More detailed examination of this interval should resolve this question. This interval coincides with a marked decrease in radiolarian preservation, which begins in Core 171B-1053-14H and culminates in Section 171B-1053-18X-CC. Radiolarian preservation increases dramatically in Core 171B-1053-19X.

PALEOMAGNETISM

Laboratory Procedures and Interpretations

Nearly all APC cores yielded apparent polarity intervals during analysis with the pass-through cryogenic magnetometer; however, these polarity zones were generally difficult to correlate between Holes 1053A and 1053B or to the magnetic polarity time scale. Paleomagnetic results from the XCB cores are compromised because of an abundance of drilling slurry between and surrounding the small biscuited segments of core. Post-cruise thermal demagnetization of 65 minicores from Hole 1053A was only partially successful in resolving the polarity zonation.

Measurements were made using the pass-through cryogenic magnetometer on the archive half of all core sections >40 cm long. Measurements were made at 4-cm intervals at natural remanent magnetization (NRM) and then either at a 15- or 20-mT alternating-field (AF) demagnetization step. The bioturbated oozes and chalks at Site 1053 commonly exhibit a significant drilling-induced overprint (radially inward and dipping steeply downward) that was partially removed by the AF demagnetization step. Discrete samples taken (typically four oriented cyclinders or plastic cubes per core) from Hole 1053A were analyzed post cruise using progressive thermal and AF demagnetization. Thermal demagnetization of 65 of these discrete minicores from Hole 1053A were completed at the paleomagnetics laboratories at the University of Oxford and the University of Michigan. These analyses and associated polarity interpretations are included in this *Initial Results* volume (see Tables 10 [ASCII format], 11 [PDF format] on CD-ROM, back pocket, this volume). Progressive thermal demagnetization was generally at 30°C increments from ~140°–360°C, with continuation to higher thermal steps for the more stable samples. A thermal demagnetization step of 200°C was generally adequate to remove overprints. Most sediments lost nearly all of their magnetization or became magnetically unstable at thermal steps exceeding 330°C.

The demagnetized data were filtered before being plotted by removing the few measurements with inclinations >80° that were assumed to be dominated by a steep-downward drilling overprint, intervals of anomalously high intensity (usually associated with fragments broken off the drill bit or rust particles within the drilling slurry), and data from the uppermost 20 cm of the disturbed top of each core. We also omitted all samples with magnetizations that were $<5 \times 10^{-3}$ mA/m after 20 mT AF demagnetization, presuming that these contain an unacceptably high component of noise. A three-point moving average was applied to the inclination record to smooth data before plotting. Other than the lower portion of each hole where XCB coring produced biscuits or blocks embedded in drilling slurry (Cores 171B-1053A-16X through 20X and 171B-1053B-15X through 20X), the polarity zonation within each hole was estimated from the clustering of shipboard inclination data and interpretation of demagnetization behavior in the discrete samples (Figs. 4, 5).

Careful cross-comparison of the data with the observed disturbances in the cored sediments and occurrences of anomalous intensity spikes would probably remove additional artifacts. However, we think it is unlikely that, before acquiring "control" data from shore-based analysis of discrete samples, further examination of the shipboard pass-through cryogenic data will significantly alter the main conclusions presented here.

Biomagnetostratigraphy

Polarity Zones and Chron Assignments

Assignment of polarity chrons to the polarity intervals relies on the shipboard micropaleontology datums (especially foraminifer and nannofossil zones) and the chronostratigraphy of Berggren et al. (1995).

Middle and Upper Eocene

The sediments cored with the APC in Holes 1053A and 1053B generally yielded similar polarity patterns (Fig. 6). The calcareous oozes in the upper 30 m yielded predominantly reversed polarity or indeterminate polarity upon thermal demagnetization, and the underlying oozes and chalks are dominated by normal polarity with a few intervals exhibiting "reversed-polarity," negative, or mixed inclinations.

One possible assignment of polarity chrons to these polarity zones that is consistent with the biostratigraphy is illustrated in Figure 6. In

Table 9. Occurrences of radiolarian taxa and relative abundances and states of faunal preservation at Hole 1053A.

Age	Zone	Core, section, interval (cm)	Depth (mbsf)	Abundance	Preservation	*Calocyclas hispida*	*Cryptocarpium azyx*	*Dictyoprora mongolfieri*	*Dictyoprora pirum*	*Eusyringium fistuligerum*	*Lychnocanoma bellum*	*Podocyrtis (Lampterium) chalara*	*Podocyrtis (Podocyrtis) papalis*	*Thyrsocyrtis (Pentalacorys) tetracantha*	*Thyrsocyrtis (Pentalacorys) triacantha*	*Thyrsocyrtis (Thyrsocyrtis) rhizodon*	*Tristylospyris triceros*	*Lychnocanoma amphitrite*	*Calocyclas turris*	*Cryptocarpium ornatum*	*Lithocyclia aristotelis group*	*Podocyrtis (Lampterium) goetheana*	*Calocyclas bandyca*	*Thyrsocyrtis (Thyrsocyrtis) bromia*	*Dictyoprora armadillo*	*Lophocyrtis (Lophocyrtis) jacchia*	*Stylatractus universus*	*Artophormis barbadensis*
		171B-1053A-																										
late Eocene	*Cryptocarpium ornatum*	1H-CC, 20-23	9.78	C	VG												R			F	C				F	F		F
late Eocene	*Cryptocarpium ornatum*	2H-CC, 29-32	19.57	A	VG			R									F			R	F				R	F		R
late Eocene	*Cryptocarpium ornatum*	3H-CC, 17-20	28.77	F	P			R												T					T	T		F
late Eocene	*Cryptocarpium ornatum*	4H-CC, 23-25	38.29	A	VG			C									R			R	F				F	F		R
late Eocene	*Cryptocarpium ornatum*	5H-CC, 21-23	47.78	A	VG			C									F			F	F				C	F		F
late Eocene	*Cryptocarpium ornatum*	6H-CC, 26-28	57.31	A	VG			C	F								R			R	F				F	F	R	
late Eocene	*Cryptocarpium ornatum*	7H-CC, 21-23	66.83	A	VG		F	A	F							C	R		F	F	F			F	C	R		
late Eocene	*Calocyclas bandyca*	8H-CC, 25-27	76.36	C	M	F		C	F				F	F	R				F	R	F		F	R	F	R		
late Eocene	*Calocyclas bandyca*	9H-CC, 12-15	85.7	C	VG	F	C	C						F		C	R		C			R	R	F				
late Eocene	*Calocyclas bandyca*	10H-CC, 0-4	94.81	A	VG	R	F	A	R				C	C	R	C	R		C	F		R	F	R				
late Eocene	*Calocyclas bandyca*	11H-CC, 24-26	104.92	F	M	F	F	C			R		F	F	R	C	R		F			R	F					
late Eocene	*Calocyclas bandyca*	12H-CC, 27-29	114.58	C	M	R	F	C	R				F	F	R	C			F	R		R						
late Eocene-middle Eocene	*Cryptocarpium azyx*	13H-CC, 12-15	123.79	A	VG	C	C	A	F	C					F	C	R		C		F	F						
late Eocene-middle Eocene	*Cryptocarpium azyx*	14H-CC, 30-32	133.46	C	P	F	F	A		F	R			F	F	F			C									
late Eocene-middle Eocene	*Cryptocarpium azyx*	15H-CC, 11-12	139.04	F	P	R		C		R						R			R									
late Eocene-middle Eocene	*Cryptocarpium azyx*	16X-CC, 15-18	147.39	F	P	F	F	F	R		R			F		F	R		R									
late Eocene-middle Eocene	*Cryptocarpium azyx*	17X-CC, 25-27	153.04	F	P	F	R	C	R	F	F			F	F	F	F			R								
late Eocene-middle Eocene	*Cryptocarpium azyx*	18X-CC, 27-29	164.03	F	M	F	R	C		F	R	R	C	R	F	F	F		T									
late Eocene-middle Eocene	*Cryptocarpium azyx*	19X-CC, 17-19	173.17	C	G	F	F	A	R	C	F	R	A	F	F	F		F										
late Eocene-middle Eocene	*Cryptocarpium azyx*	20X-CC, 39-41	183.31	F	M	C	C	C	F	F	R	T	C	F	F	F	R											

Notes: Abundance: C = common; A = abundant; F = few; R = rare; T = trace. Preservation: VG = very good; P = poor; M = moderate; G = good.

Berggren et al.'s (1995) chronostratigraphy for the late Eocene, foraminifer Zone P16 spans polarity Chron C13r through the upper part of Chron C15r, which is an interval dominated by reversed polarity (Fig. 6). Following thermal demagnetization, there is a predominance of reversed polarity in the upper 30 m of Hole 1053A. We assign this interval to Chron C13r in the upper part of foraminifer Zone P16. The AF demagnetization of the same interval in the shipboard measurements was inadequate to resolve this zone (e.g., Hole 1053B in Fig. 6). Chron C15n extends downward to ~50–55 mbsf, where a poorly defined zone of possible reversed polarity near the base of foraminifer Zone P16 may be Chron C15r. The assignment of the base of nannofossil Zone CP15 to ~160 mbsf in each hole implies that the main normal-polarity zone is equivalent to Chrons C16n and C17n, with reversed-polarity Chron C16r tentatively assigned to a poorly resolved feature at about 147 mbsf. The underlying reversed-polarity interval below 160 mbsf is tentatively correlated with Chron C17r.

In contrast to similar upper Eocene oozes and chalks at other sites drilled during Leg 171B, this facies at Site 1053 did not yield a reliable magnetostratigraphy using the pass-through magnetometer, even when augmented by thermal demagnetization of minicores.

CORE-CORE INTEGRATION

At Site 1053, magnetic susceptibility and GRAPE density data from the MST and output from the Minolta color spectrophotometer were available for precise core-core correlation (Tables 12, 13 on CD-ROM, back pocket, this volume). Two holes, 1053A and 1053B, were cored with the APC, and a composite section was attempted to the limit of parallel APC coring, at about 133 mbsf (Table 14).

Correlating the two holes at Site 1053 proved surprisingly difficult, and it is most likely that an improved composite section will emerge from post-cruise analysis. There were two reasons for the difficulties encountered. First, the magnetic susceptibility data are apparently not as reliable as data from Site 1052; the measurements drifted during the run of individual sections in a manner that gives one cause for concern about using small variations in susceptibility for correlation purposes. Second, the cores were generally greenish but mottled with brown spots, resulting in a color output from the spectrophotometer that is noisy and, once again, prejudices its reliability for correlation. The data are shown vs. composite depth (mcd) in Figures 7 through 13. Figure 7 shows a good example of the difficulty regarding the magnetic susceptibility data; the two holes are presumably tightly tied by the prominent color change at about 13 mcd, yet the susceptibility data at that depth differ greatly between the two holes. Figure 10 illustrates the reverse situation: the two cores are well tied at about 72 mcd by the prominent spike in magnetic susceptibility that was caused by an ash layer, yet the color data match poorly.

The overlap between the cores in the parallel holes is good; for example, in Figure 10 the spike caused by the ash layer at about 72 mcd is in Sections 171B-1053A-8H-2 and 1053B-8H-5. Thus, even where the composite section we constructed is poorly justified, it is most likely that a complete record was recovered. Although splice tie points are listed in Table 15, it is advisable for high-resolution sampling to extend outside the limits given for the splice at points where the ties are poorly constrained.

ORGANIC GEOCHEMISTRY

Gas Analyses

In Hole 1053A, gas chromatographic analysis of the headspace samples detected small volumes of methane (C_1) with a trace occurrence of ethane (C_2; Table 16). At the only occurrence of C_2 (0.6 ppm) at 80.5 mbsf, the C_1/C_2 ratio of 23 was in the potentially hazardous range of <100 (Table 16). No restriction on drilling activities was necessary because the total gas content remained below 0.01 vol% C_1. Because no hazardous levels of gas were detected in Hole 1053A, gases were not monitored in Hole 1053B.

Two gas zones, each containing only small volumes of methane, were recognized in Hole 1053A (Fig. 14). The surface gas zone is

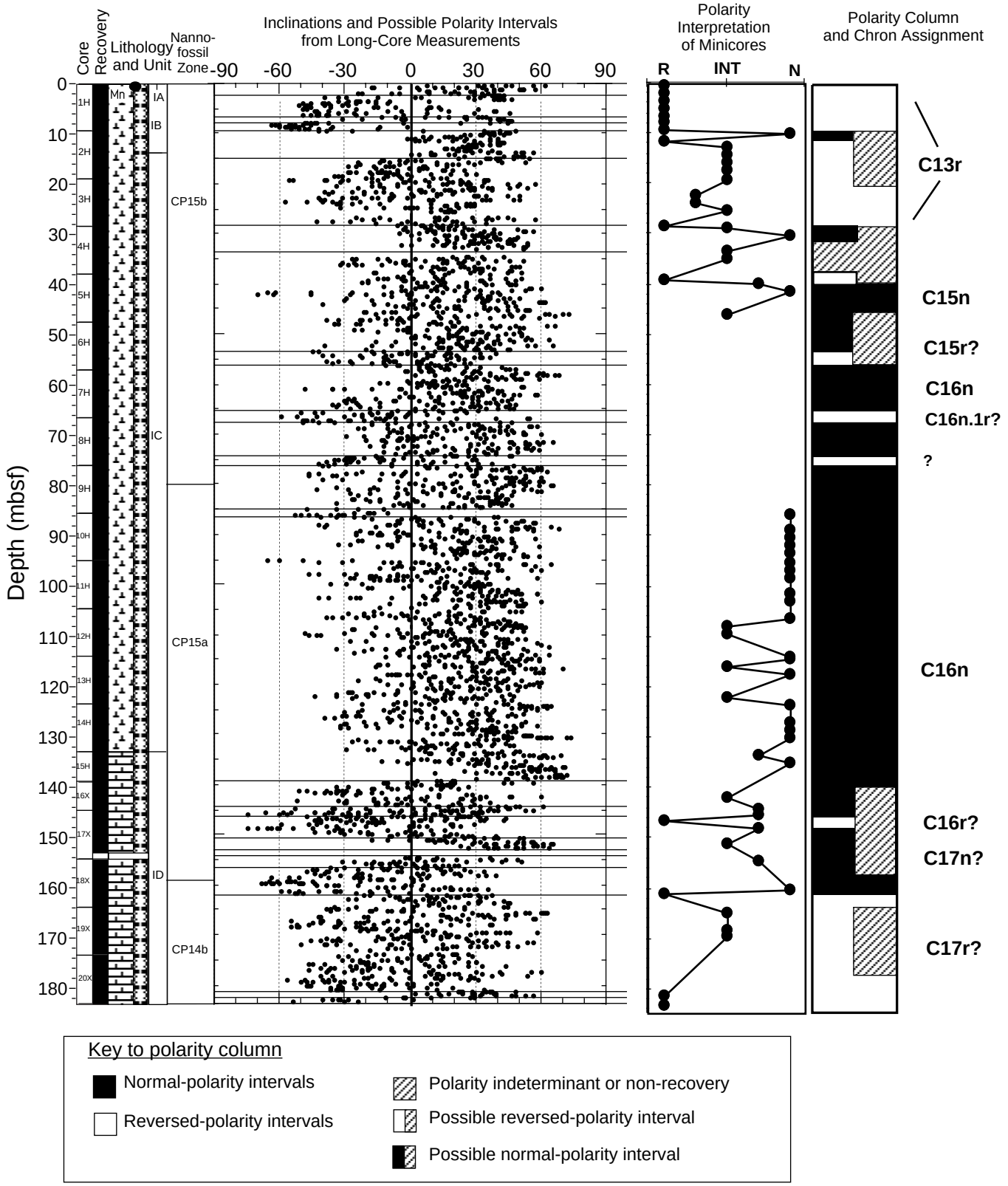

Figure 4. Magnetostratigraphy of Hole 1053A. Magnetic inclinations from long-core measurements are after AF demagnetization at 20 mT and were filtered using a three-point moving average. Measurements from the uppermost 20 cm of each core and those having anomalously high or low magnetic intensities were removed. Horizontal lines delineate clusters of predominantly positive, negative, or equally mixed magnetic inclinations that were used for a preliminary shipboard polarity column. Polarity of discrete minicores are from interpretation of progressive thermal demagnetization and are assigned relative degrees of certainty. These polarity interpretations from discrete samples are given priority in the compilation of the summary polarity column. Polarity chron assignments are based on the polarity zone pattern and nannofossil biostratigraphy.

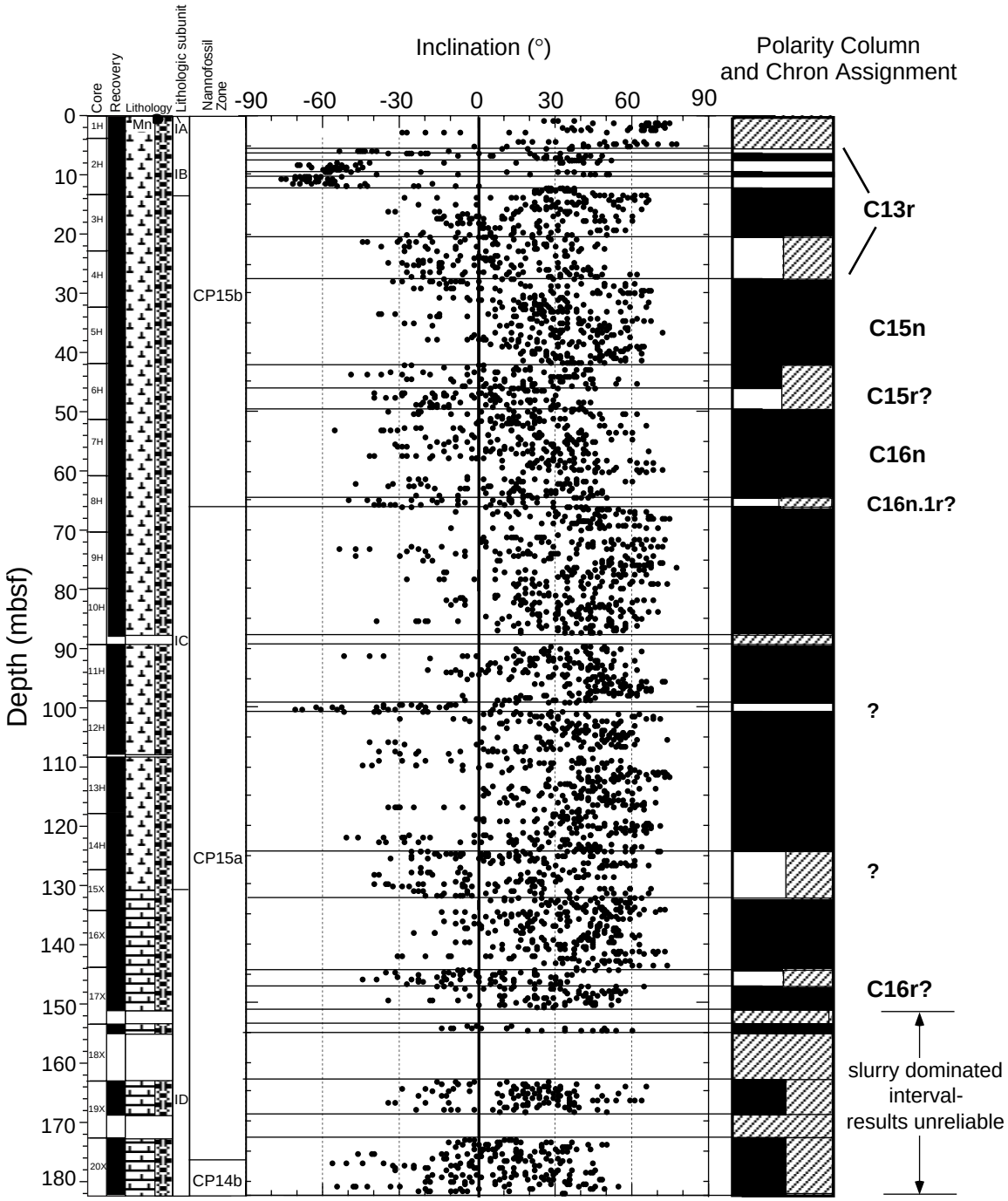

Figure 5. Magnetostratigraphy of Hole 1053B. Magnetic inclinations from long-core measurements are after AF demagnetization at 20 mT and were filtered using a three-point moving average. Measurements from the uppermost 20 cm of each core and those having anomalously high or low magnetic intensities were removed. Horizontal lines delineate clusters of predominantly positive, negative, or equally mixed magnetic inclinations that were used for a preliminary shipboard polarity column. Polarity chron assignments are based on correlation to polarity zones at similar depths in Hole 1053A and on nannofossil biostratigraphy.

from 4.5 to 139 mbsf in lithologic Subunits IB and IC. The surface gas zone averages 10 ppm C_1 and shows a generally increasing gas content of 2 to 20 ppm C_1 with depth. The transition from lithologic Subunit IC to Subunit ID at 139 mbsf forms the upper boundary of the deep gas zone, which is marked by a sharp drop in the C_1 content from 20 to 13 ppm. After this sharp drop in gas content, C_1 content steadily increases again, reaching 16 ppm at the bottom of the hole at 183 mbsf (Fig. 14). Overall, the gas content of the deep gas zone is low, averaging only 12 ppm C_1 and ranging from 8 to 16 ppm C_1.

Elemental Analyses

Three samples were taken from each core for carbonate-carbon and total carbon, hydrogen, nitrogen, and sulfur (CHNS) analyses. In

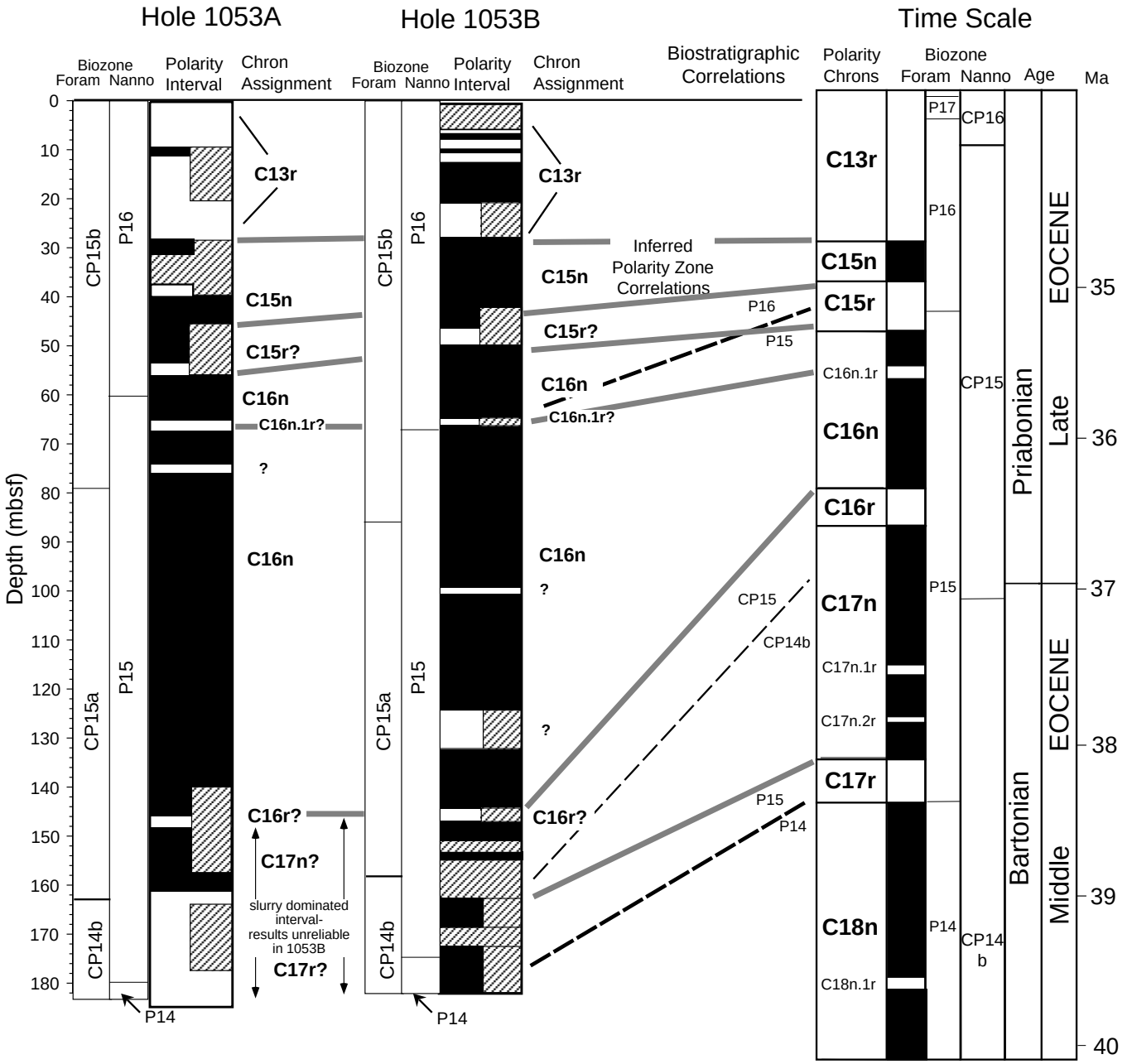

Figure 6. Comparison of polarity zonations from the two holes at Site 1053 with Paleogene chronostratigraphy. Thermal demagnetization of discrete minicores in Hole 1053A resolved reversed-polarity zones, whereas the AF demagnetization of cores in Hole 1053B was inadequate to remove secondary normal-polarity overprints. Biostratigraphic correlations = dashed lines; possible assignment of polarity chrons = thick lines.

Hole 1053A, carbonate averages 75 wt% and varies little with depth (Fig. 15). The uniform carbonate content is consistent with the single lithologic unit described at Site 1053. Total organic carbon (TOC) content of all samples is below the detection limit of 0.3 wt% (Table 17; Fig. 16). Sulfur, which usually accompanies organic matter in small amounts, was not detected at Site 1053 (Table 17).

The hydrogen content was also low, averaging 0.26 wt% and ranging from 0.16 to 0.41 wt%. Hydrogen does not vary much with depth (Fig. 16) and may represent a constant low background level of kerogen deposition, which carries much of the hydrogen in sediment.

Detectable levels of nitrogen occurs only sporadically in the sediments (Fig. 16). The nitrogen content is low, averaging 0.03 wt% and ranging from below detection limit to 0.39 wt%. The variation of nitrogen content may represent the sporadic deposition or preservation of marine kerogen, which carries much of the nitrogen in sediment.

INORGANIC GEOCHEMISTRY

Analytical Results

Interstitial waters were taken from 11 core samples at Site 1053 (Holes 1053A and 1053B; Table 18). Pore-water salinities at this site show little variation (Fig. 17A). Pore-water chloride values show a slight increase from near-seawater concentrations (556 mM) at the top of the section to 569 mM at ~33 mbsf, followed by a slight de-

Table 14. Offsets applied to the depths (mbsf) of individual cores at Site 1053 to generate a composite section and a composite depth scale (mcd).

Core	Offset (m)
171B-1053A-	
1H	0.20
2H	−0.30
3H	0.05
4H	0.45
5H	0.35
6H	1.54
7H	1.54
8H	3.10
9H	3.22
10H	3.22
11H	3.64
12H	4.34
13H	4.68
14H	5.94
15H	5.94
16X	5.94
17X	5.94
18X	5.94
19X	5.94
20X	5.94
171B-1053B-	
1H	0.00
2H	0.10
3H	0.15
4H	1.10
5H	2.15
6H	2.49
7H	3.14
8H	4.48
9H	4.40
10H	4.46
11H	6.16
12H	6.16
13H	7.22
14H	7.56
15X	7.68
16X	7.68
17X	7.68
18X	7.68
19X	7.68
20X	7.68

crease at ~40 mbsf (Fig. 17B). Below this depth, chloride values are nearly constant to the bottom of the hole (Fig. 17B). Pore-water sodium concentrations range between 475 and 485 mM, and the depth profile is similar to the chloride profile (Fig. 17B).

Pore-water alkalinity shows a steady increase from ~3 mM at the top of the section to 6.68 mM at 161.75 mbsf (Fig. 17C). The pH of pore waters shows a slight overall decrease (7.64–7.37) with depth (Fig. 17C).

Pore-water calcium concentrations are always higher than standard seawater (10.55 mM) and increase steadily from a minimum of 10.93 mM in the shallowest sample (4.45 mbsf) to 19.97 mM at 180.15 mbsf (Fig. 17A). Magnesium concentrations are always lower than standard seawater (54 mM) and decrease steadily from a maximum of 53.47 mM in the shallowest sample to 46.76 mM over the same depth range (Fig. 17A).

Pore-water potassium concentrations show an increase from a near-seawater concentration at the top of the section (11 mM) to a peak of 13.1 mM at ~33 mbsf (Fig. 17D). Below this depth, potassium concentrations show an overall decrease to ~10 mM at the base of the section. Pore-water rubidium concentrations at Site 1053 are always greater than seawater concentration (1.4 µM), and the depth profile is remarkably similar to the potassium profile (Fig. 17E, D, respectively).

Pore-water strontium concentrations are always higher than standard seawater (90 µM), and they increase steadily from a minimum of 95 µM in the shallowest sample (4.45 mbsf) to 400 µM at the base of the section (Fig. 17F). Calculated Sr/Ca values show a similar pattern to the strontium concentration depth profile (Fig. 17G, F, respectively). Pore-water lithium concentrations also increase steadily with depth (from a value near seawater at the top of the section to 169 µM at the base of the section; Fig. 17F).

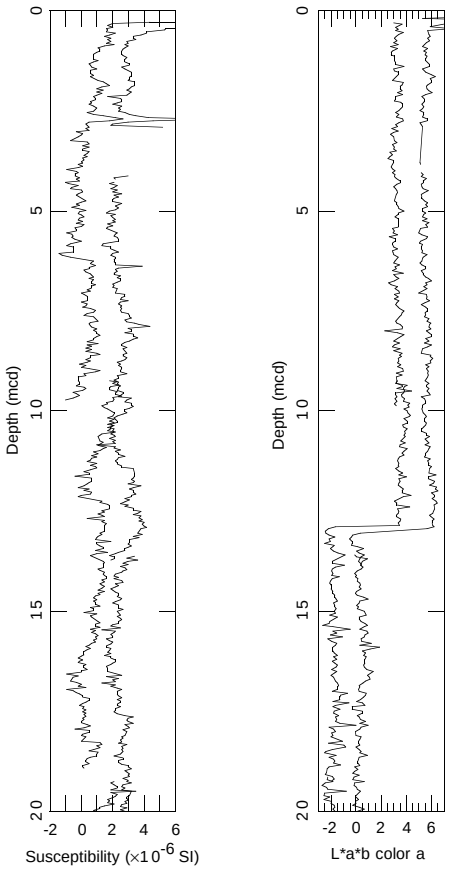

Figure 7. Magnetic susceptibility data and L*a*b code a from 0 to 20 mcd in Holes 1053A and 1053B. The magnetic susceptibility and color data are available on CD-ROM (back pocket, this volume).

Pore-water dissolved silica concentrations show a general increase with depth from~ 600 µM at the top of the section to ~1000 µM at the base of the section (Fig. 17H).

Pore-water sulfate concentrations show a slight overall decrease in value from near-seawater concentrations in the upper 30 m of the section to 25.7 mM at the bottom of the section (Fig.17I). Pore-water ammonium concentrations show a steady increase with depth from ~10 µM near the top of the section to 326 µM at ~180 mbsf (Fig.17I).

Discussion

The interstitial pore-water chemistry at Site 1053 is similar to the chemistry at the other Leg 171B sites on the Blake Nose. However, depth gradients (to ~150 mbsf) in pore-water calcium, magnesium, strontium, and lithium concentrations at Site 1053 are steeper than those at the other Blake Nose sites, except for the fact that the strontium gradients from Sites 1053 and 1052 are virtually identical. Sedimentation rates at Site 1053 are approximately double the rates at Site 1052 (see “Biostratigraphy” section in this chapter and in the “Site 1052” chapter, this volume). Therefore, sedimentation rates cannot account for the fact that Site 1053 chemical gradients are generally steeper than those at the other sites on the Blake Nose.

PHYSICAL PROPERTIES

Physical properties at Site 1053 were measured on both whole-round sections and discrete samples from split-core sections. Whole-round measurements included the determination of GRAPE bulk density, magnetic susceptibility, and thermal conductivity. Index

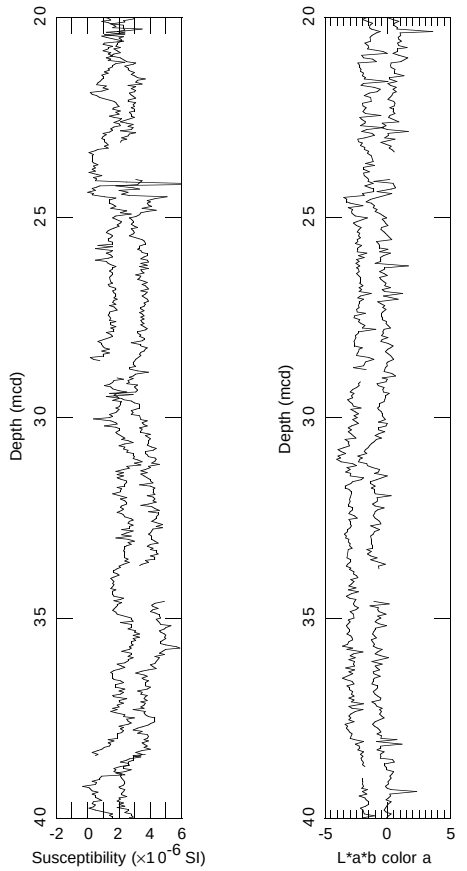

Figure 8. Magnetic susceptibility data and L*a*b code a from 20 to 40 mcd in Holes 1053A and 1053B. The magnetic susceptibility and color data are available on CD-ROM (back pocket, this volume).

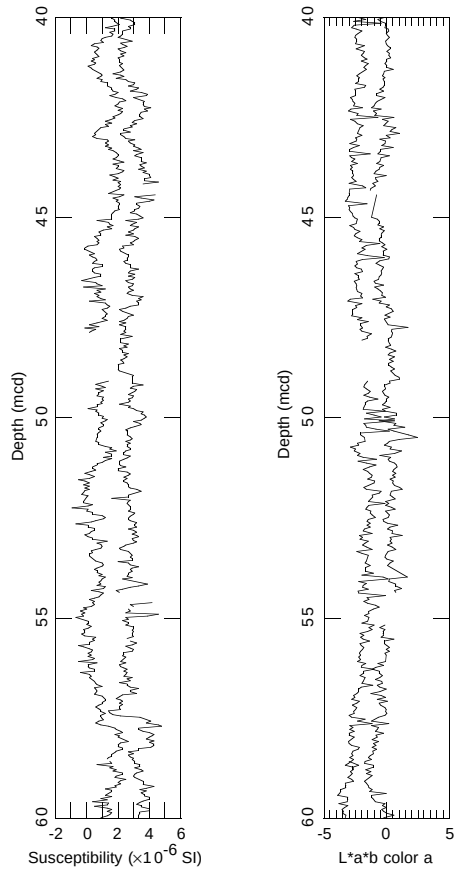

Figure 9. Magnetic susceptibility data and L*a*b code a from 40 to 60 mcd in Holes 1053A and 1053B. The magnetic susceptibility and color data are available on CD-ROM (back pocket, this volume).

properties, *P*-wave velocity, shear strength, and resistivity were measured on discrete samples from split-core sections at a frequency of three measurements per core. Except for *P*-wave velocity, discrete physical properties data are not available for the interval between 50 and 85 mbsf because the possible occurrence of Eocene tektites precluded sampling of these cores. MST *P*-wave velocity and natural gamma radiation were not measured at Site 1053 because of the limited time available before beginning operations in Hole 1050C.

MST Measurements

GRAPE data were filtered to remove anomalous values that are artifacts of section-end and void or crack effects. The data set was filtered to remove values outside the 10% error band of a reference curve, which was calculated from a 10-point running mean of the data. This filtering of the data set significantly improves visual presentation and aids data interpretation.

GRAPE bulk density was measured on all cores from Site 1053 (Fig. 18; Tables 19, 20 on CD-ROM, back pocket, this volume). These data, along with magnetic susceptibility and color reflectance, were used to form a Site 1053 composite stratigraphic section (see "Core-Core Integration" section, this chapter).

GRAPE bulk density shows an increase in magnitude from 1.55 to 1.9 g/cm^3 from 0 to 140 mbsf in Hole 1053A. A similar increase in GRAPE bulk density, from 1.6 to 1.87 g/cm^3, is also observed between 0 and 127 mbsf in Hole 1053B. At 140 mbsf in Hole 1053A and 127 mbsf in Hole 1053B, a sharp decrease in bulk density corresponds with the ooze to chalk transition between lithologic Subunits IC and ID in these two holes (see "Lithostratigraphy" section, this chapter). GRAPE bulk density increases in magnitude after this sharp decrease across an ~5-m-thick interval in both holes to values of about 1.85 g/cm^3. From 145 mbsf in Hole 1053A and from 132 mbsf in Hole 1053B to total depth, bulk density fluctuates about an approximate average of 1.8 g/cm^3.

MST measurements of magnetic susceptibility from Holes 1053A and 1053B are shown in Figure 19 (also see Tables 21, 22 on CD-ROM, back pocket, this volume). Throughout Holes 1053A and 1053B, magnetic susceptibility fluctuates at about background levels, with distinct magnetic susceptibility "spikes," some of which correlate with ash layers.

Index Properties

Index properties were determined for Hole 1053A (Table 23; Fig. 20). Index properties data suggest that progressive sediment compaction and fluid expulsion with depth are the dominant factors contributing to the physical nature of the sediments. Bulk and dry density values show a steady increase in magnitude between the seafloor and 140 mbsf, from average values of 1.6 to 1.9 g/cm^3 and 0.94 to 1.44 g/cm^3, respectively. The observed maxima of bulk and dry densities at 140 mbsf occur at the ooze to chalk transition. Below 140 mbsf, in lithologic Subunit ID, bulk and dry densities decrease to 1.8 and 1.25 g/cm^3, respectively. Within lithologic Subunit ID, grain density is lower than that measured above 140 mbsf, suggesting that the observed changes below 140 mbsf may reflect a composition change, such as increased siliceous content, as well as diagenetic changes at the ooze to chalk transition.

Sediment porosity, water content, and void ratio (Fig. 20) show complementary inverse trends with depth to those observed for bulk and dry densities. Porosity, water content, and void ratio all show

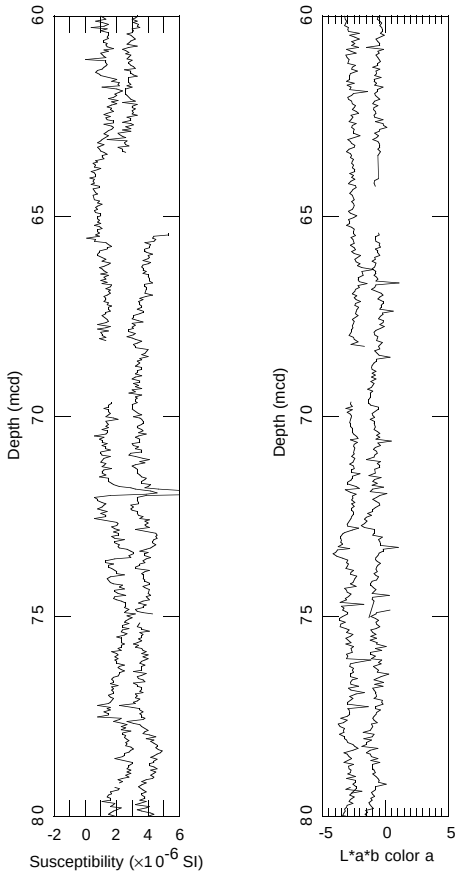

Figure 10. Magnetic susceptibility data and L*a*b code a from 60 to 80 mcd in Holes 1053A and 1053B. The magnetic susceptibility and color data are available on CD-ROM (back pocket, this volume).

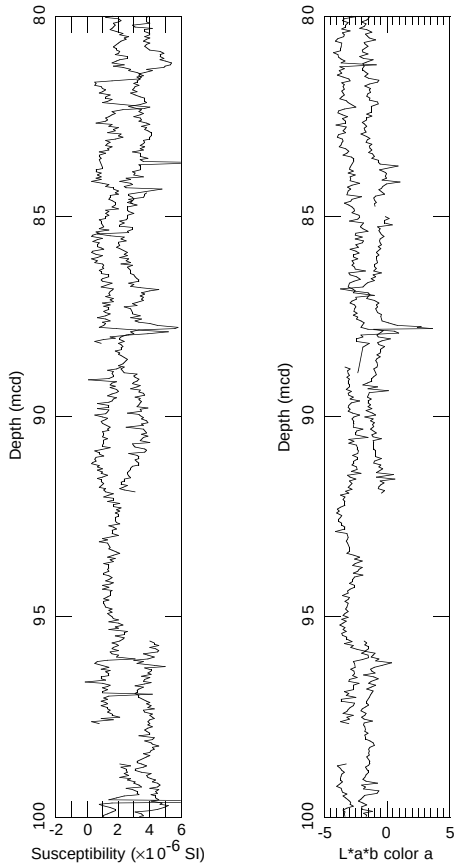

Figure 11. Magnetic susceptibility data and L*a*b code a from 80 to 100 mcd in Holes 1053A and 1053B. The magnetic susceptibility and color data are available on CD-ROM (back pocket, this volume).

minima at the ooze to chalk transition at 140 mbsf. Below 140 mbsf, these properties show a stepped increase that may be caused by a compositional change coincident with the ooze to chalk transition.

Discrete bulk density measurements show good agreement with GRAPE bulk density estimates for the interval cored with both APC and XCB (between 0 and 180 mbsf) in Hole 1053A (Fig. 21).

P-wave Velocity

Discrete measurements of *P*-wave velocity were obtained on split-core sections from Hole 1053A using the Hamilton Frame velocimeter (Table 24; Fig. 22). *P*-wave velocity shows a general increase with depth from 1.56 km/s at the seafloor to 1.8 km/s at 180 mbsf, with three data points of significantly higher velocity. These higher velocity measurements may be the consequence of greater amounts of lithification. The last APC core in Hole 1053A, which extended to 139 mbsf, had an extremely short stroke, suggesting that a hard layer exists at this depth. Two of the higher velocity values were measured in samples from between 139 and 142 mbsf. Between 0 and 125 mbsf, velocity shows a linear increase from 1.56 to 1.62 km/s. No change in velocity is observed across the contact between lithologic Subunits IB and IC, which is defined by a color change. An increase in velocity occurs across the ooze to chalk transition at 140 mbsf, which defines the contact between lithologic Subunits IC and ID. The observed positive relationship between velocity and bulk density (Fig. 23) supports the notion of increased cementation across the ooze to chalk transition, although the clustering of data points at ~1.85 g/cm^3 and 1.75 km/s, respectively, probably reflects a compositional influence in lithologic Subunit ID. Cementation would increase velocity and bulk densities through the addition of secondary carbonate. Between 140 and 180 mbsf, *P*-wave velocity values are generally between 1.64 and 1.8 km/s.

Undrained Shear Strength

Undrained shear strength was measured on sediments recovered from Hole 1053A using both the miniature vane-shear device and, when the sediment became too indurated to insert the vane-shear device, a pocket penetrometer (Table 25; Fig. 24). There is no well-defined relationship between shear strength and depth in Hole 1053A, although there is a slight apparent increase downhole. Pocket penetrometer measurements are biased toward values higher than those obtained with the vane-shear device.

Normalized shear strength, the ratio of shear strength (S_u) to effective overburden pressure (P_0'), can be used to assess the stress history of a sediment column. Normalized shear strength ratios (S_u/P_0') determined for Hole 1053A are plotted against depth in Figure 25. A normally consolidated sediment has an S_u/P_0' between 0.2 and 0.22 (Ladd et al., 1977). Sediments measured with the vane-shear apparatus above 18 mbsf in Hole 1053A have $S_u/P_0' > 0.22$ and are overconsolidated. Below 18 mbsf in Hole 1053A, S_u/P_0' for sediments measured with the vane-shear apparatus are generally ≤0.2, suggesting that sediments below this depth are underconsolidated. S_u/P_0' calculated using pocket penetrometer shear strength measurements are considered overestimates of the actual normalized shear strength. Assuming that the sediment at 0.79 mbsf where the maximum value of S_u was measured was normally consolidated at maximum overburden thickness and that no changes in shear strength have occurred, esti-

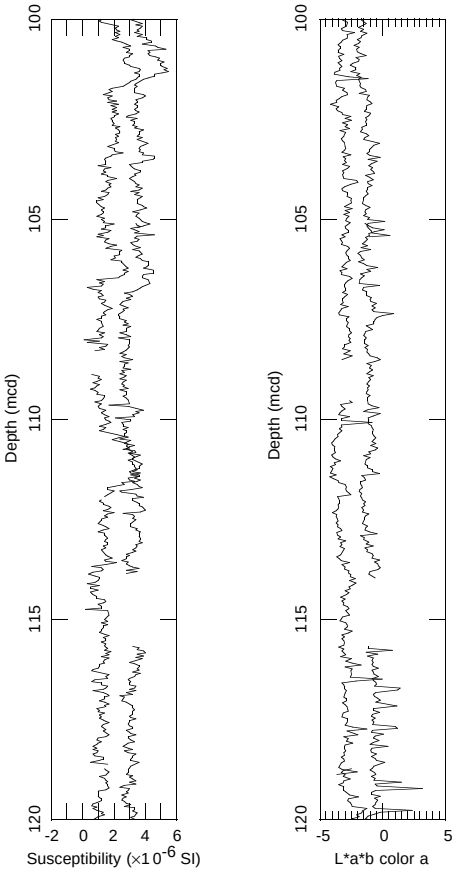

Figure 12. Magnetic susceptibility data and L*a*b code a from 100 to 120 mcd in Holes 1053A and 1053B. The magnetic susceptibility and color data are available on CD-ROM (back pocket, this volume).

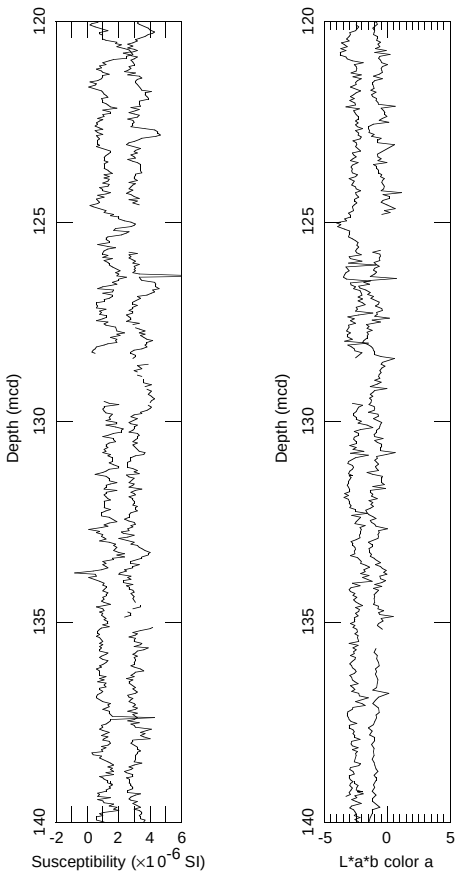

Figure 13. Magnetic susceptibility data and L*a*b code a from 120 to 140 mcd in Holes 1053A and 1053B. The magnetic susceptibility and color data are available on CD-ROM (back pocket, this volume).

Table 15. Splice table for Site 1053.

Hole, core, section, interval (cm)	Depth (mbsf)	Depth (mcd)	Whether tied	Hole, core, section, interval (cm)	Depth (mbsf)	Depth (mcd)
171B-						
1053B-1H-1, 0-0	0	0	Start	171B-		
1053B-1H-2, 61.00-61.00	2.11	2.11	Tie to	1053A-1H-2, 41.00-41.00	1.91	2.11
1053A-1H-4, 33.00-33.00	4.83	5.03	Tie to	1053B-2H-1, 102.00-102.00	4.93	5.03
1053B-2H-7, 13.00-13.00	13.03	13.13	Tie to	1053A-2H-3, 93.00-93.00	13.43	13.13
1053A-2H-4, 145.00-145.00	15.45	15.15	Tie to	1053B-3H-2, 8.50-8.50	15.00	15.15
1053B-3H-6, 61.00-61.00	21.51	21.66	Tie to	1053A-3H-2, 110.00-110.00	21.61	21.66
1053A-3H-5, 105.00-105.00	26.05	26.10	Tie to	1053B-4H-2, 59.50-59.50	25.00	26.10
1053B-4H-6, 37.00-37.00	30.77	31.87	Tie to	1053A-4H-2, 140.50-140.50	31.42	31.87
1053A-4H-5, 125.00-125.00	35.75	36.20	Tie to	1053B-5H-2, 14.00-14.00	34.05	36.20
1053B-5H-6, 125.00-125.00	41.15	43.30	Tie to	1053A-5H-4, 45.00-45.00	42.95	43.30
1053A-5H-6, 65.00-65.00	46.15	46.50	Tie to	1053B-6H-2, 61.00-61.00	44.01	46.50
1053B-6H-7, 5.00-5.00	50.95	53.44	Tie to	1053A-6H-3, 139.50-139.50	51.90	53.44
1053A-6H-6, 25.00-25.00	55.25	56.79	Tie to	1053B-7H-2, 74.00-74.00	53.65	56.79
1053B-7H-5, 73.00-73.00	58.13	61.27	Tie to	1053A-7H-2, 122.00-122.00	59.73	61.27
1053A-7H-6, 77.00-77.00	65.27	66.81	Tie to	1053B-8H-1, 142.00-142.00	62.33	66.81
1053B-8H-6, 5.00-5.00	68.45	72.93	Tie to	1053A-8H-3, 33.00-33.00	69.83	72.93
1053A-8H-6, 117.00-117.00	75.17	78.27	Tie to	1053B-9H-3, 46.00-46.00	73.87	78.27
1053B-9H-6, 49.00-49.00	78.39	82.79	Tie to	1053A-9H-3, 57.00-57.00	79.57	82.79
1053A-9H-5, 117.00-117.00	83.17	86.39	Tie to	1053B-10H-2, 53.00-53.00	81.93	86.39
1053B-10H-4, 53.00-53.00	84.93	89.39	Tie to	1053A-10H-1, 66.00-66.00	86.17	89.39
1053A-10H-5, 109.00-109.00	92.59	95.81	Tie to	1053B-11H-1, 25.00-25.00	89.65	95.81
1053B-11H-6, 89.00-89.00	97.79	103.95	Tie to	1053A-11H-4, 81.00-81.00	100.31	103.95
1053A-11H-6, 85.00-85.00	103.35	106.99	Tie to	1053B-12H-2, 42.00-42.00	100.83	106.99
1053B-12H-6, 21.00-21.00	106.61	112.77	Tie to	1053A-12H-3, 93.00-93.00	108.43	112.77
1053A-12H-6, 73.00-73.00	112.73	117.07	Tie to	1053B-13H-1, 145.00-145.00	109.85	117.07
1053B-13H-6, 13.00-13.00	116.03	123.25	Tie to	1053A-13H-4, 6.00-6.00	118.57	123.25
1053A-13H-5, 113.00-113.00	121.13	125.81	Tie to	1053B-14H-1, 34.00-34.00	118.25	125.81
1053B-14H-6, 77.00-77.00	126.17	133.73	Tie to	1053A-14H-3, 129.00-129.00	127.79	133.73
1053A-14H-7, 57.00-57.00	133.07	139.01	Tie to	1053A-15H-1, 6.00-6.00	133.07	139.01
1053A-15H-4, 137.00-137.00	138.87	144.81	End			

Table 16. Hole 1053A headspace gas composition.

Core, section, interval (cm)	Depth (mbsf)	Gas zone	C_1 (ppm)	C_2 (ppm)	C_2= (ppm)	C_1/C_2
171B-1053A-						
1H-4, 0-5	4.5	Surface	2.1			
2H-4, 0-5	14.0	Surface	2.3			
3H-4, 0-5	23.5	Surface	3.4			
4H-4, 0-5	33.0	Surface	4.7			
5H-4, 0-5	42.5	Surface	4.3			
6H-4, 0-5	52.0	Surface	6.1			
7H-4, 0-5	61.5	Surface	8.3			
8H-4, 0-5	71.0	Surface	12.0			
9H-4, 0-5	80.5	Surface	14.0	0.6		23.3
10H-4, 0-5	90.0	Surface	10.4			
11H-4, 0-5	99.5	Surface	10.1			
12H-4, 0-5	109.0	Surface	14.0			
13H-4, 0-5	118.5	Surface	16.7			
14H-4, 0-5	128.0	Surface	14.6			
15H-4, 0-5	137.5	Surface	20.4			
16X-4, 0-5	143.5	Deep	8.2			
17X-4, 0-5	149.2	Deep	10.9			
18X-4, 0-5	158.8	Deep	11.1			
19X-4, 0-5	168.4	Deep	12.6			
20X-4, 0-5	178.0	Deep	16.2			

Notes: In all cases, the injected sample size was 5 cm^3. Concentration of gas is in parts per million by volume. Where no values are reported, concentrations are below detection limits.

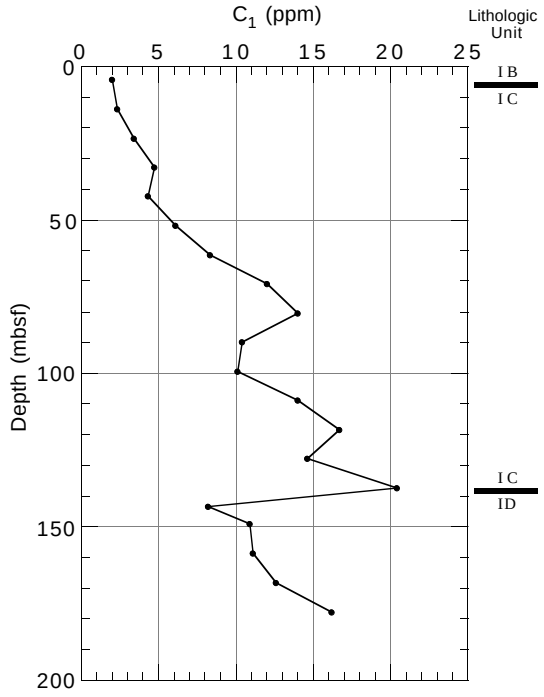

Figure 14. Methane (C_1) content vs. depth in Hole 1053A. Lithologic units are described in the "Lithostratigraphy" section (this chapter).

mation of the overburden thickness suggests that as little as 3.8 m of sediment may have accumulated in and been removed at Hole 1053A between the late Eocene and present.

Resistivity

The resistivity data from Hole 1053A were measured using the Scripps Institution of Oceanography probe (Table 26; Fig. 26). Between 0 and 135 mbsf, resistivity shows a general increase in magnitude from 0.43 to 0.77 Ωm. Below 125 mbsf, resistivity increases from ~0.65 Ωm to values between 0.7 and 0.77 Ωm. This increase in

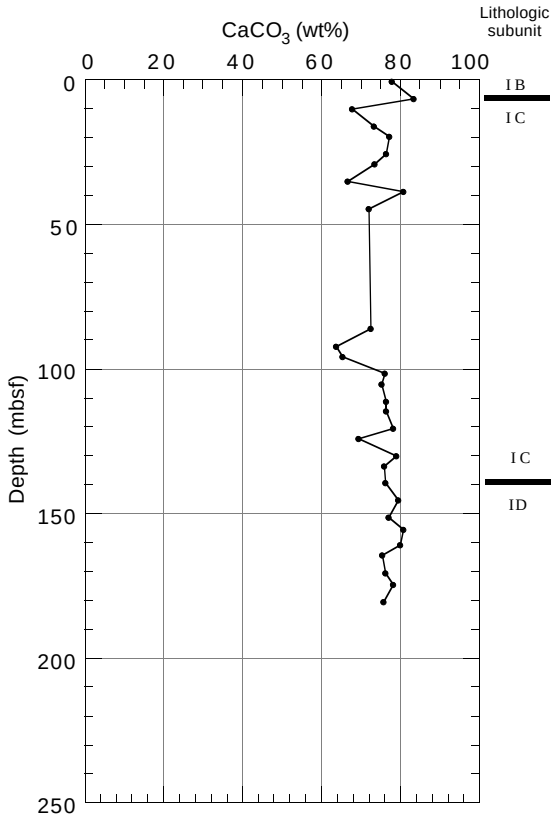

Figure 15. Carbonate content vs. depth in Hole 1053A. Lithologic units are described in the "Lithostratigraphy" section (this chapter).

resistivity is most likely related to cementation processes associated with the ooze to chalk transition. This notion is supported by the negative correlation between resistivity and porosity (Fig. 27), which indicates that a decrease in porosity increases resistivity, possibly because of secondary carbonate cementation.

Thermal Conductivity

Thermal conductivity data from the APC cores of Hole 1053B are listed in Table 27 and are shown in Figure 28. Thermal conductivity measurements for Hole 1053B were obtained using the TK-04 instrument, and they display the most well-defined depth trend for data collected during Leg 171B. Six measurements of <0.8 W/(m·K) may be spurious data points resulting from poor thermal contact between the needle probe and the sediment during data collection. Thermal conductivity shows a generally linear increase in magnitude between the seafloor and 125 mbsf, from 1.05 to 1.3 W/(m·K). The average thermal conductivity for the depth interval 0–125 mbsf (excluding the six anomalous data points) is 1.17 ± 0.16 W/(m·K).

Summary

Physical properties data indicate that compaction and fluid expulsion, as well as physicochemical changes related to the ooze to chalk transition, are the controlling factors on sediment properties. Over the entire sampled interval, sediment lithification influences velocity and resistivity by decreasing the *P*-wave traveltime across grain contacts and by decreasing porosity, respectively. Physical properties show discontinuities across the ooze to chalk transition at 140 mbsf. Higher bulk density and velocity measurements in this transition zone suggest that greater amounts of lithification have occurred in this inter-

Table 17. Hole 1053A total inorganic carbon, carbonate, total carbon, total organic carbon, nitrogen, sulfur, and hydrogen analyses.

Core, section, interval (cm)	Depth interval (mbsf)	TIC (wt%)	$CaCO_3$ (wt%)	TC (wt%)	TOC (wt%)	N (wt%)	S (wt%)	H (wt%)
171B-1053A-								
1H-1, 77-78	0.77-0.78	9.33	77.71	9.43	0.10			0.20
1H-5, 74-75	6.74-6.75	10.00	83.27	10.06	0.06			0.19
2H-1, 78-79	10.28-10.29	8.14	67.80	8.27	0.13			0.31
2H-5, 77-78	16.27-16.28	8.80	73.28	9.04	0.24			0.33
3H-1, 77-78	19.77-19.78	9.25	77.07	9.41	0.16			0.29
3H-5, 77-78	25.77-25.78	9.17	76.36	9.39	0.22	0.29		0.28
4H-1, 77-78	29.27-29.28	8.82	73.45	9.04	0.22	0.39		0.31
4H-5, 78-79	35.28-35.29	7.99	66.54	8.12	0.13			0.39
5H-1, 77-78	38.77-38.78	9.69	80.68	9.80	0.11	0.08		0.23
5H-5, 72-73	44.72-44.73	8.63	71.93	8.73	0.10			0.29
10H-1, 78-79	86.28-86.29	8.70	72.43	8.84	0.14	0.09		0.29
10H-5, 78-79	92.28-92.29	7.65	63.70	7.71	0.06			0.41
11H-1, 78-79	95.78-95.79	7.83	65.24	7.88	0.05			0.39
11H-5, 78-79	101.78-101.79	9.12	75.96	9.28	0.16			0.24
12H-1, 95-96	105.45-105.46	9.02	75.18	9.11	0.09			0.27
12H-5, 80-81	111.30-111.31	9.15	76.25	9.20	0.05			0.23
13H-1, 78-79	114.78-114.79	9.16	76.28	9.36	0.20			0.26
13H-5, 78-79	120.78-120.79	9.37	78.03	9.51	0.14	0.07		0.23
14H-1, 77-78	124.27-124.28	8.33	69.40	8.47	0.14			0.39
14H-5, 79-80	130.29-130.30	9.48	78.94	9.62	0.14			0.23
15H-1, 78-79	133.78-133.79	9.10	75.80	9.25	0.15	0.06		0.27
16X-1, 55-56	139.55-139.56	9.15	76.18	9.15	0.00			0.18
16X-5, 47-48	145.47-145.48	9.54	79.46	9.61	0.07			0.18
17X-5, 77-79	151.47-151.49	9.24	77.00	9.33	0.09			0.22
18X-1, 136-137	155.66-155.67	9.69	80.72	9.76	0.07			0.16
18X-5, 78-79	161.08-161.09	9.58	79.80	9.62	0.04			0.20
19X-1, 70-71	164.60-164.61	9.05	75.42	9.02	0.00	0.04		0.22
19X-5, 81-82	170.71-170.72	9.13	76.08	9.14	0.01			0.22
20X-1, 128-128.5	174.78-174.79	9.38	78.17	9.41	0.03			0.21
20X-5, 129-130	180.79-180.80	9.07	75.58	9.16	0.09			0.24

Notes: TIC = total inorganic carbon; TC = total carbon; TOC = total organic carbon computed by difference (TC – TIC). Negative TOC values are reported as 0.00. wt% = weight percent. Where no values are reported, concentrations are below detection limits. The gap in the data represents Cores 171B-1053A-6H through 9H (47.5–85.5 mbsf) that were not sampled.

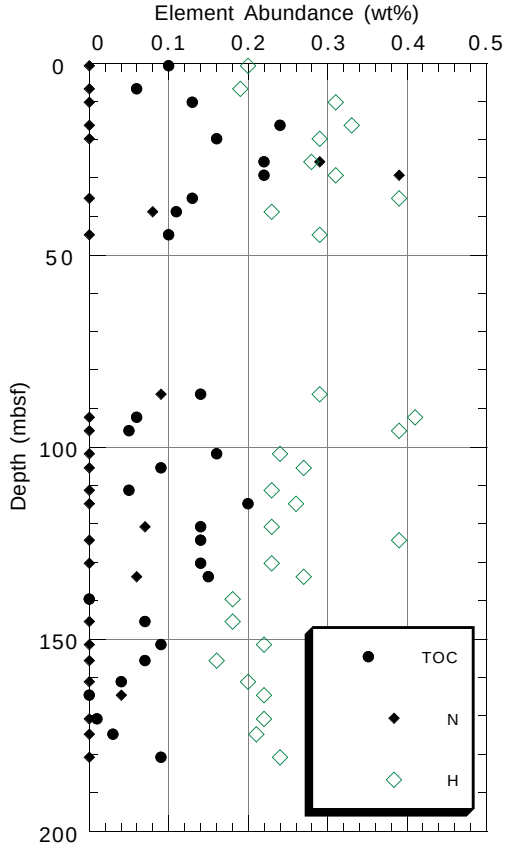

Figure 16. Elemental abundance and TOC vs. depth in Hole 1053A. The gap in the data represents Cores 171B-1053A-6H through 9H (47.5–85.5 mbsf), which were not sampled. Lithologic units are described in the "Lithostratigraphy" section (this chapter).

val. Grain density data indicate that in addition to diagenetic changes, the ooze to chalk transition at 140 mbsf may be influenced by a change in sediment composition. Sediment porosity decreases significantly at the ooze to chalk transition and abruptly increases below this interval.

HEAT FLOW AND IN SITU TEMPERATURE MEASUREMENTS

The Adara tool was run three times in the upper section of Hole 1053B (Table 28) to measure in situ temperature until sediment conditions prevented further measurements. In contrast to Site 1051, in situ temperature at Site 1053 increases linearly with depth, which suggests that in this region of the seafloor, a one-dimensional conductive heat-flow model is appropriate (Fig. 29). The geothermal gradient calculated from these measurements is 17.1°C/km (r^2 = 0.955). Heat flow computed for this site using the measured geothermal gradient and the average of laboratory-determined thermal conductivity measurements of the sediments (1.17 W/m·K; see "Physical Properties" section, this chapter) is 19.0 mW/m^2. Hole 1053B is located above a 9-km-thick sequence of carbonate platform sediments deposited on Mesozoic rift-stage basement (Dillon and Popenoe, 1988). The heat-flow value obtained for Hole 1053B is consistent with this geologic context. Published heat-flow values for sites north and east of Hole 1053B are significantly higher. Henderson and Davis (1983) estimated heat flow in the Blake-Bahama Basin to be between 42 and 57 mW/m^2 (Deep Sea Drilling Project Site 534), and Ruppel et al. (1995) obtained heat-flow values between 46 and 48.4 mW/m^2 on the Blake Outer Ridge and the Carolina Rise area. Higher heat flow in these areas is a consequence of their proximity to oceanic crust.

REFERENCES

Berggren, W.A., Kent, D.V., Swisher, C.C., III, and Aubry, M.-P., 1995. A revised Cenozoic geochronology and chronostratigraphy. *In* Berggren, W.A., Kent, D.V., Aubry, M.-P., and Hardenbol, J. (Eds.), *Geochronol-*

ogy, Time Scales and Global Stratigraphic Correlation. Spec. Publ.—Soc. Econ. Paleontol. Mineral., 54:129–212.

Clymer, A.K., Bice, D.M., and Montanari, A., 1996. Shocked quartz from the late Eocene: impact evidence from Massignano, Italy. *Geology,* 24:483–486.

Dillon, W.P., and Popenoe, P., 1988. The Blake Plateau basin and Carolina Trough. *In* Sheridan, R.E., and Grow, J.A. (Eds.), *The Atlantic Continental Margin, U.S.,* Geol. Soc. Am., Geology of North America, I-2:291–328.

Henderson, J., and Davis, E.E., 1983. An estimate of the heat flow in the western North Atlantic at Deep Sea Drilling Project Site 534. *In* Sheridan, R.E., Gradstein, F.M., et al., *Init. Repts. DSDP,* 76: Washington (U.S. Govt. Printing Office), 719–724.

Ladd, D.D., Foott, R., Ishihara, K., Schlosser, F., and Poulos, H.G., 1977. Stress-deformation and strength characteristics: state-of-the-art report. *Proc. 9th Int. Conf. Soil Mechanics Foundation Engineering,* Tokyo, 2:421–482.

Ruppel, C., Von Herzen, R.P., and Bonneville, A., 1995. Heat flux through an old (~175 Ma) passive margin: offshore southeastern United States. *J. Geophys. Res.,* 100:20037–20057.

Sanfilippo, A., Riedel, W.R., Glass, B.P., and Kyte, F.T., 1985. Late Eocene microtektites and radiolarian extinctions on Barbados. *Nature,* 314:613–615.

Saunders, J.B., Bernoulli, D., Mueller-Merz, E., Oberhänsli, H., Perch-Nielsen, K., Riedel, W.R., Sanfilippo, A., and Torrini, R., Jr., 1984. Stratigraphy of the late middle Eocene to early Oligocene in the Bath Cliff section Barbados, West Indies. *Micropaleontology,* 30:390–425.

Ms 171BIR-107

NOTE: Core-description forms ("barrel sheets") and core photographs can be found in Section 4, beginning on page 363. Forms containing smear-slide data can be found on CD-ROM. See Table of Contents for material contained on CD-ROM.

Table 18. Interstitial-water geochemical data for Site 1053.

Core, section, interval (cm)	Depth (mbsf)	pH	Alkalinity (mM)	Salinity (g/kg)	Cl (mM)	Na (mM)	Mg (mM)	Ca (mM)	SO_4 (mM)	NH_4 (μM)	H_4SiO_4 (μM)	K (mM)	Sr (μM)	Li (μM)	Rb (μM)
171B-1053A-															
1H-3, 145-150	4.45	7.64	2.97	35.0	556	475	53.47	10.93	27.9	12	591	11.0	95	32	2.00
2H-3, 145-150	13.95	7.59	3.51	36.0	558	478	52.83	11.56	28.7	8	705	12.3	104	39	2.21
3H-3, 145-150	23.45	7.55	4.00	36.0	562	481	53.02	12.75	29.0	24	658	11.8	123	46	2.08
4H-3, 145-150	32.95	7.79	4.18	36.0	569	485	51.89	13.24	27.8	49	714	13.1	129	52	2.38
5H-3, 145-150	42.45	7.41	4.60	36.0	562	479	51.96	14.13	28.5	61	765	12.4	154	59	2.24
6H-3, 145-150	51.95	7.38	4.82	35.5	564	480	51.42	14.60	27.4	77	836	11.3	166	70	2.18
9H-3, 145-150	80.45	7.41	5.56	36.0	566	480	50.03	16.45	26.7	144	754	11.7	208	92	2.23
12H-3, 145-150	108.95	7.30	5.98	36.0	569	485	48.43	17.73	26.6	187	840	10.9	254	116	2.18
15X-2, 145-150	137.45	7.26	6.78	35.5	567	479	47.38	19.19	24.6	256	825	10.7	305	136	2.23
18X-5, 145-150	161.75	7.37	6.68	36.0	567	481	47.16	19.97	25.7	293	981	9.8	345	158	2.04
171B-1053B-															
20X-5, 145-150	180.15			36.0	563		46.76	19.97	25.7	326		9.9	401	169	1.98

Note: Where no values are reported, data are absent.

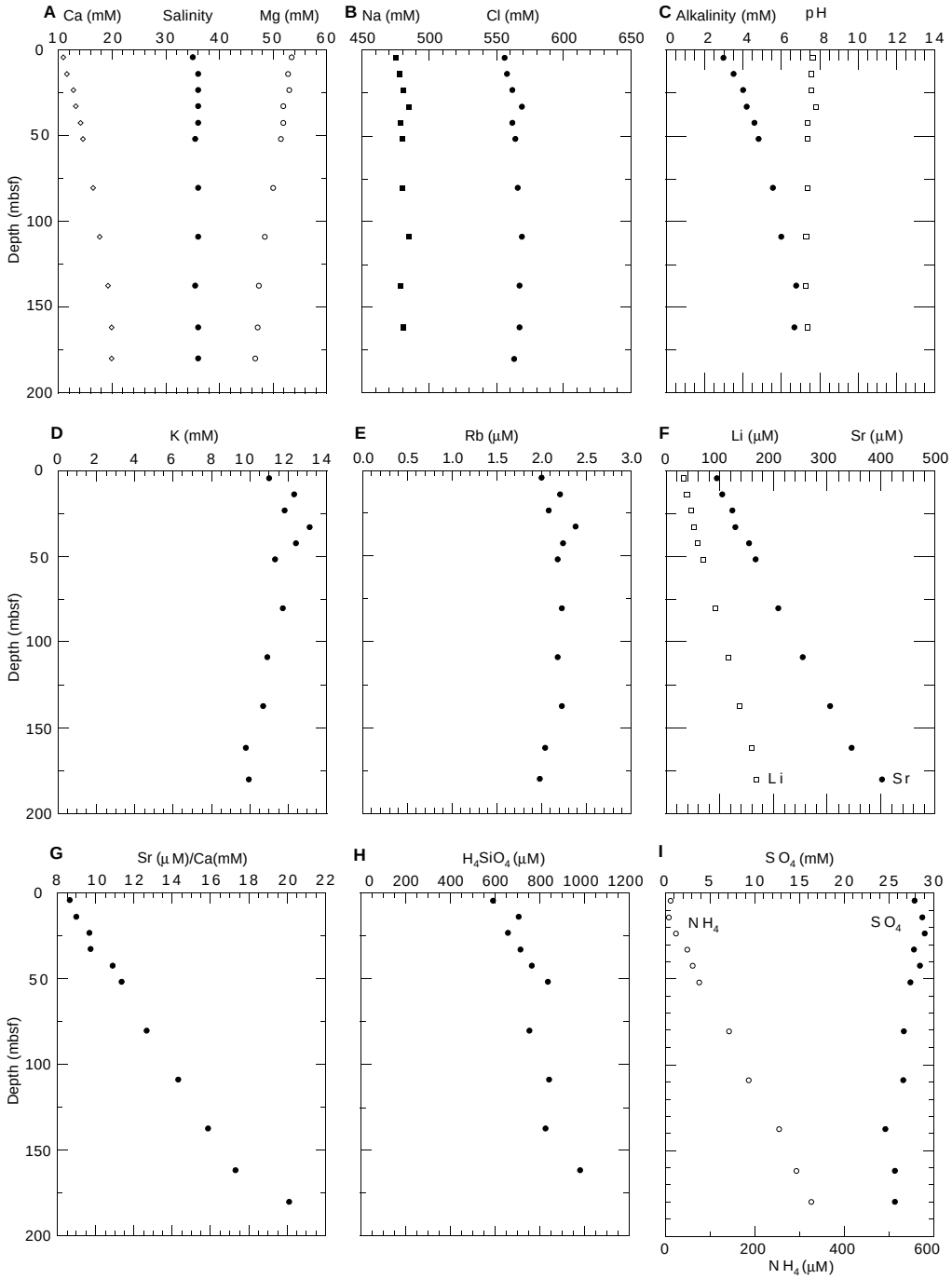

Figure 17. Interstitial-water geochemical data for Hole 1053A vs. depth. **A.** Calcium, salinity, and magnesium. **B.** Sodium and chloride. **C.** Alkalinity and pH. **D.** Potassium. **E.** Rubidium. **F.** Lithium and strontium. **G.** Strontium/calcium ratio. **H.** Silica. **I.** Sulfate and ammonium.

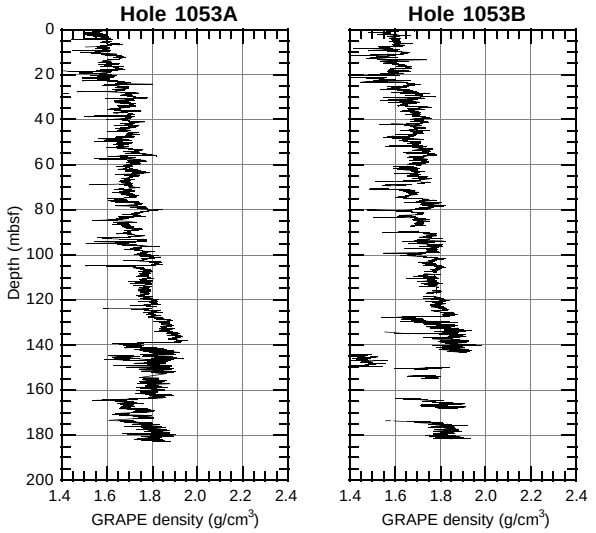

Figure 18. GRAPE bulk density for Holes 1053A and 1053B (also see Tables 19, 20 [CD-ROM, back pocket, this volume] for data).

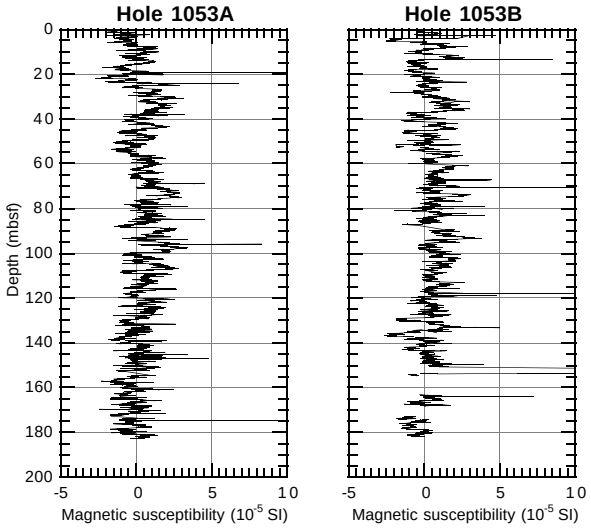

Figure 19. Magnetic susceptibility for Holes 1053A and 1053B (also see Tables 21, 22 [CD-ROM, back pocket, this volume] for data).

Table 23. Discrete index properties measurements for Hole 1053A.

Core, section, interval (cm)	Depth (mbsf)	Water content (total mass wt%)	Water content (solid mass wt%)	Bulk density (g/cm^3)	Grain density (g/cm^3)	Dry density (g/cm^3)	Porosity (%)	Void ratio
171B-1053A-								
1H-1, 74-76	0.74	69.7	41.1	1.61	2.66	0.95	64.4	1.81
1H-3, 74-76	3.74	67.7	40.4	1.63	2.70	0.97	64.1	1.78
1H-5, 70-72	6.70	64.4	39.2	1.64	2.67	1.00	62.7	1.68
2H-1, 75-77	10.25	82.9	45.3	1.54	2.63	0.84	68.1	2.13
2H-3, 54-56	13.04	61.2	37.9	1.65	2.64	1.02	61.2	1.58
2H-5, 74-76	16.24	63.8	39.0	1.64	2.66	1.00	62.4	1.66
3H-1, 75-77	19.75	74.2	42.6	1.58	2.65	0.91	65.7	1.92
3H-3, 77-79	22.77	68.4	40.6	1.61	2.64	0.96	63.8	1.76
3H-5, 74.5-76.5	25.75	58.3	36.8	1.67	2.65	1.06	60.2	1.51
4H-1, 73.5-75.5	29.24	53.9	35.0	1.70	2.65	1.11	58.3	1.40
4H-3, 75-77	32.25	58.6	36.9	1.67	2.66	1.06	60.3	1.52
4H-5, 75-77	35.25	64.5	39.2	1.63	2.64	0.99	62.4	1.66
5H-1, 74-76	38.74	55.9	35.8	1.69	2.65	1.08	59.1	1.44
5H-3, 74.5-76.5	41.75	55.0	35.5	1.69	2.64	1.09	58.6	1.42
5H-5, 69-71	44.69	56.2	36.0	1.69	2.66	1.08	59.3	1.46
10H-1, 75-77	86.25	58.3	36.8	1.67	2.62	1.05	59.9	1.49
10H-3, 75-77	89.25	51.7	34.1	1.72	2.65	1.13	57.2	1.34
10H-5, 75-77	92.25	59.3	37.2	1.66	2.64	1.04	60.4	1.53
12H-1, 92-94	105.42	52.0	34.2	1.71	2.63	1.13	57.2	1.33
12H-3, 78-80	108.28	47.7	32.3	1.75	2.64	1.18	55.2	1.23
12H-5, 78-80	111.28	45.3	31.2	1.77	2.65	1.22	53.9	1.17
13H-1, 75-77	114.75	47.4	32.2	1.75	2.64	1.19	55.0	1.22
13H-3, 75-77	117.75	46.3	31.6	1.77	2.66	1.21	54.6	1.20
13H-5, 75-77	120.75	44.0	30.6	1.78	2.65	1.24	53.3	1.14
14H-1, 78-80	124.28	49.3	33.0	1.73	2.63	1.16	55.8	1.27
14H-3, 78-80	127.28	43.4	30.3	1.79	2.66	1.25	53.0	1.13
14H-5, 77-79	130.27	39.6	28.3	1.82	2.64	1.31	50.4	1.02
15H-1, 75-77	133.75	38.0	27.5	1.84	2.63	1.33	49.4	0.98
15H-3, 75-77	136.75	34.0	25.4	1.89	2.66	1.41	46.9	0.88
16X-1, 53-55	139.53	33.0	24.8	1.90	2.64	1.43	46.0	0.85
16X-3, 73-75	142.73	38.7	27.9	1.84	2.66	1.33	50.2	1.01
16X-5, 45-47	145.45	38.6	27.8	1.83	2.64	1.32	49.8	0.99
17X-1, 36-38	145.06	38.6	27.9	1.83	2.63	1.32	49.8	0.99
17X-3, 58-60	148.28	37.9	27.5	1.85	2.66	1.34	49.5	0.98
17X-5, 54-56	151.24	38.5	27.8	1.83	2.64	1.32	49.8	0.99
18X-1, 136-138	155.66	39.6	28.3	1.82	2.61	1.30	50.2	1.01
18X-2, 95-97	156.75	42.8	30.0	1.78	2.61	1.25	52.2	1.09
18X-4, 77-79	159.57	41.1	29.1	1.81	2.64	1.28	51.5	1.06
18X-5, 75-77	161.05	43.1	30.1	1.79	2.63	1.25	52.6	1.11
19X-1, 68-70	164.58	40.7	28.9	1.80	2.60	1.28	50.8	1.03
19X-3, 87-89	167.77	37.2	27.1	1.84	2.62	1.34	48.7	0.95
19X-4, 74-76	169.14	37.0	27.0	1.84	2.62	1.35	48.6	0.95
19X-6, 95.5-97.5	172.36	38.9	28.0	1.81	2.58	1.30	49.4	0.98
20X-1, 129-131	174.79	45.2	31.1	1.77	2.64	1.22	53.8	1.17
20X-3, 114-116	177.64	40.8	29.0	1.81	2.62	1.28	51.0	1.04
20X-5, 127-129	180.77	39.5	28.3	1.81	2.60	1.30	50.1	1.01

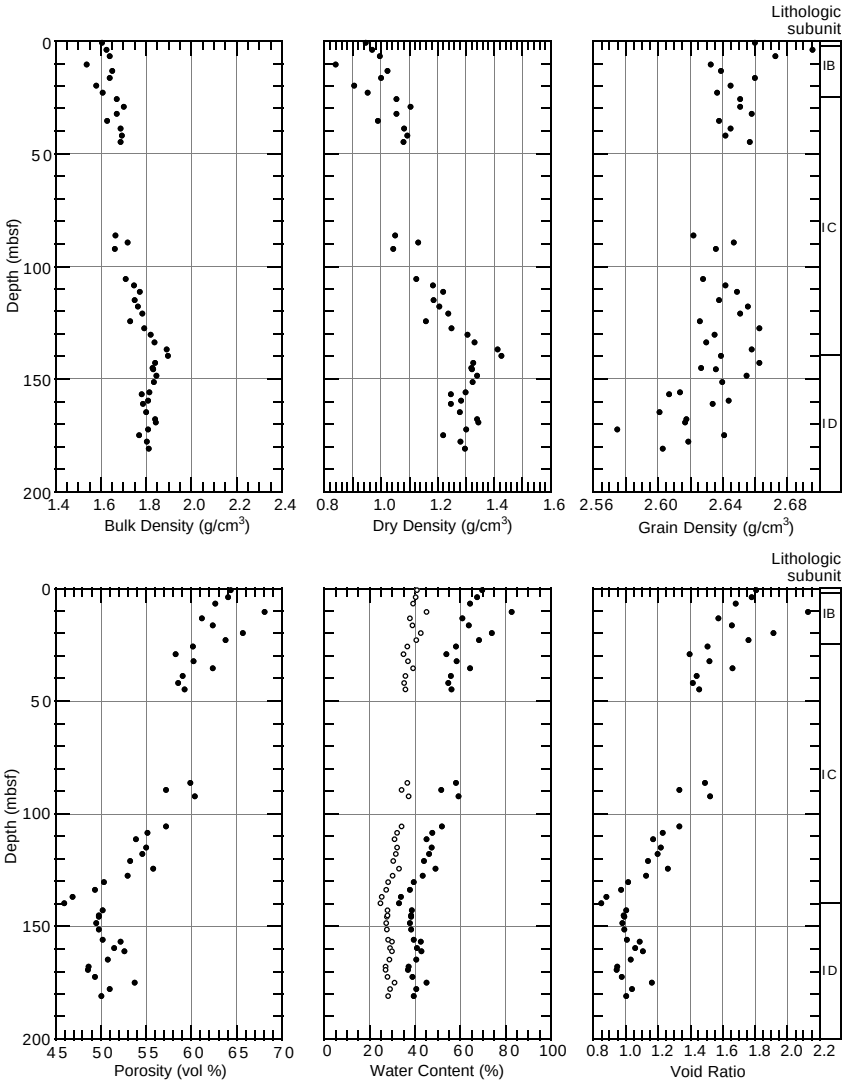

Figure 20. Discrete measurements of bulk, dry, and grain densities, porosity, water content, and void ratio for Hole 1053A. Lithologic units (see “Lithostratigraphy” section, this chapter) are included for comparative purposes. In the water content plot, open circles = values expressed in terms of total mass; solid circles = values expressed in terms of the total mass of solids.

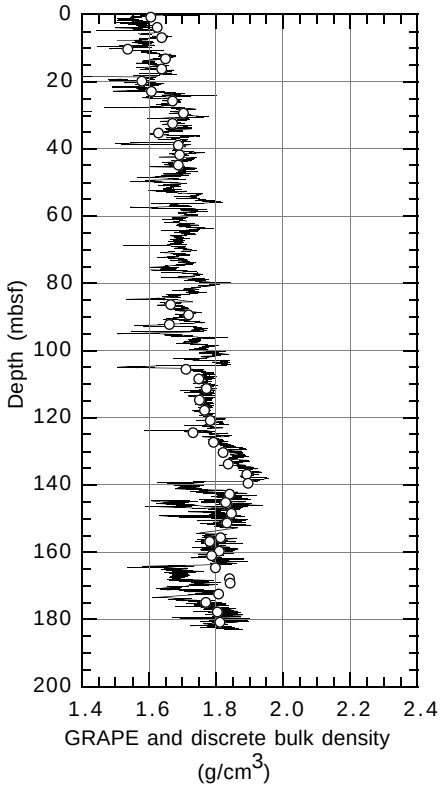

Figure 21. Comparison of composite GRAPE bulk density (line) with discrete measurements of bulk density (open circles) for Hole 1053A.

Table 24. Discrete measurements of uncorrected transverse *P*-wave velocity for Hole 1053A.

Core, section, interval (cm)	Depth (mbsf)	Transverse *P*-wave velocity (km/s)
171B-1053A-		
1H-1, 74-76	0.74	1.568
1H-3, 74.2-76.2	3.74	1.561
1H-5, 70-72	6.70	1.561
2H-1, 74-76	10.24	1.547
2H-3, 48.1-50.1	12.98	1.562
2H-5, 74-76	16.24	1.563
3H-1, 74-76	19.74	1.553
3H-3, 76.8-78.8	22.77	1.567
3H-5, 73.9-75.9	25.74	1.569
4H-1, 74-76	29.24	1.593
4H-3, 74-76	32.24	1.575
4H-5, 73.9-75.9	35.24	1.577
5H-1, 74-76	38.74	1.583
5H-3, 74-76	41.74	1.573
5H-5, 68.7-70.7	44.69	1.578
6H-1, 74-76	48.24	1.571
6H-3, 73.3-75.3	51.23	1.584
6H-5, 73.9-75.9	54.24	1.581
7H-1, 74-76	57.74	1.592
7H-3, 74-76	60.74	1.571
7H-5, 11.5-13.5	63.12	1.589
8H-1, 74-76	67.24	1.583
8H-3, 74-76	70.24	1.583
8H-5, 74-76	73.24	1.604
9H-1, 67.8-69.8	76.68	1.584
9H-3, 73.9-75.9	79.74	1.621
9H-5, 67.1-69.1	82.67	1.588
10H-1, 74.1-76.1	86.24	1.585
10H-3, 62.6-64.6	89.13	1.596
10H-5, 74-76	92.24	1.600
11H-1, 74-76	95.74	1.601
11H-3, 74-76	98.74	1.616
11H-5, 73.9-75.9	101.74	1.607
12H-1, 92.3-94.3	105.42	1.586
12H-3, 74.1-76.1	108.24	1.607
12H-5, 74.1-76.1	111.24	1.634
13H-1, 74-76	114.74	1.622
13H-3, 74-76	117.74	1.611
13H-5, 74-76	120.74	1.624
14H-1, 78.3-80.3	124.28	1.617
14H-3, 56.9-58.9	127.07	1.631
14H-5, 74-76	130.24	1.643
15H-1, 74-76	133.74	1.656
15H-3, 74-76	136.74	1.672
16X-1, 54.8-56.8	139.55	1.800
16X-3, 72.7-74.7	142.73	2.297
16X-5, 46-48	142.46	1.677
17X-1, 65.1-67.1	145.35	1.705
17X-3, 58.7-60.7	148.29	1.734
17X-5, 56-58	151.26	1.789
18X-1, 21.6-23.6	154.52	1.758
18X-5, 109.3-111.3	161.39	1.743
19X-1, 59-61	164.49	1.951
19X-3, 74-76	167.64	1.727
19X-5, 79.4-81.4	170.69	1.771
20X-1, 128.7-130.7	174.79	1.648
20X-3, 113.3-115.3	177.63	1.752
20X-5, 126-128	180.76	1.784

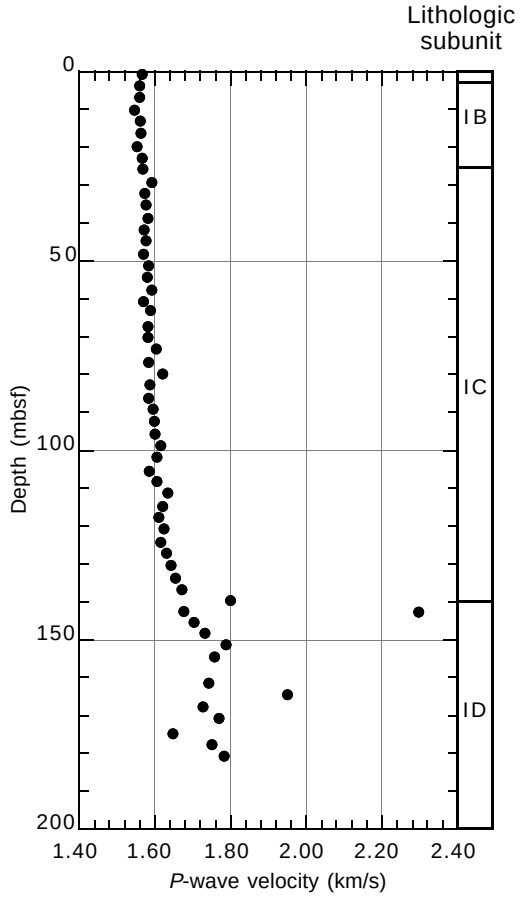

Figure 22. Discrete *P*-wave velocity for Hole 1053A. Lithologic units (see "Lithostratigraphy" section, this chapter) are included for comparative purposes.

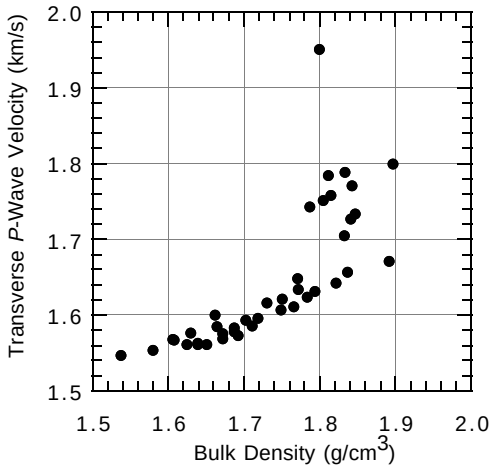

Figure 23. Comparison of discrete transverse *P*-wave velocity and discrete bulk density for Hole 1053A. The *P*-wave velocity values are uncorrected for in situ pressure and temperature conditions.

Table 25. Discrete measurements of shear strength for Hole 1053A.

Core, section, interval (cm)	Depth (mbsf)	Peak (kPa)	Residual (kPa)	Penetrometer (kPa)
171B-1053A-				
1H-1, 78.6-80.6	0.79	53.46	26.91	
1H-3, 78.2-80.2	3.78	18.29	11.52	
1H-5, 75.8-77.8	6.76	27.05	13.53	
2H-1, 78.2-80.2	10.28	71.85	31.62	
2H-3, 52.6-54.6	13.03	49.78	29.20	
2H-5, 80.4-82.4	16.30	65.47	31.64	
3H-1, 79.3-81.3	19.79	29.43	11.58	
3H-3, 80.1-82.1	22.80	39.07	17.19	
3H-5, 84.9-86.9	25.85	65.14	30.18	
4H-1, 77.1-79.1	29.27	64.50	31.60	
4H-3, 71.8-73.8	32.22	115.14	21.49	
4H-5, 76-78	35.22			103.0
5H-1, 72.6-74.6	38.73			46.6
5H-3, 76-78	41.75			95.6
5H-5, 72-74	44.71			115.2
10H-1, 79-81	86.28			110.3
10H-3, 79-81	89.28			120.1
10H-5, 79-81	92.28			>220.6
11H-1, 71-73	95.70			188.8
11H-2, 71-73	97.20			166.7
11H-3, 71-73	98.70			132.4
11H-4, 69-71	100.18			191.2
11H-5, 72-74	101.71			218.2
11H-6, 74-76	103.23			154.5
12H-1, 95-97	105.44			110.3
12H-2, 79-81	106.78			205.9
12H-3, 79-81	108.28			144.7
12H-4, 79-81	109.78			>220.6
12H-5, 79-81	111.28			>220.6
13H-1, 80-82	114.79			144.7
13H-2, 79-81	116.28			93.2
13H-3, 79-81	117.78			176.5
14H-1, 79-81	124.28			149.6
14H-3, 79-81	127.28			127.5
14H-5, 79-81	130.28			>220.6
15H-1, 79-81	133.78			171.6
15H-3, 79-81	136.78			142.2

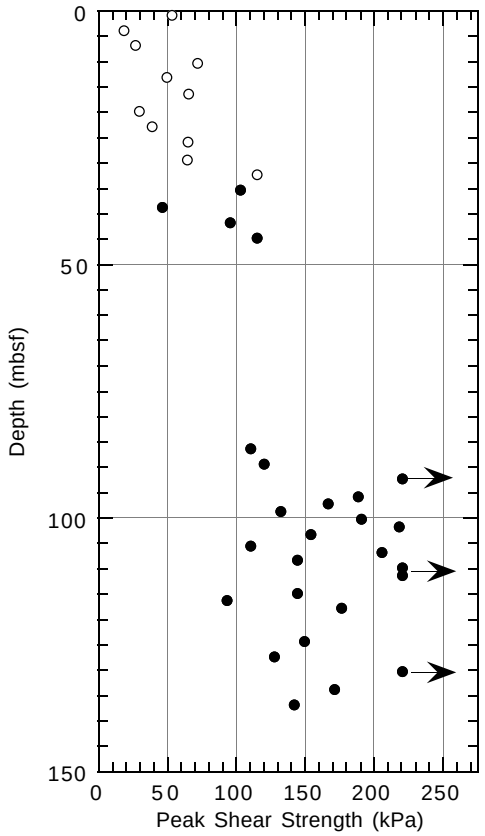

Figure 24. Shear strength for Hole 1053A. Open circles = vane-shear device measurements; solid circles = pocket penetrometer measurements; arrows = measurements in excess of the range of the pocket penetrometer.

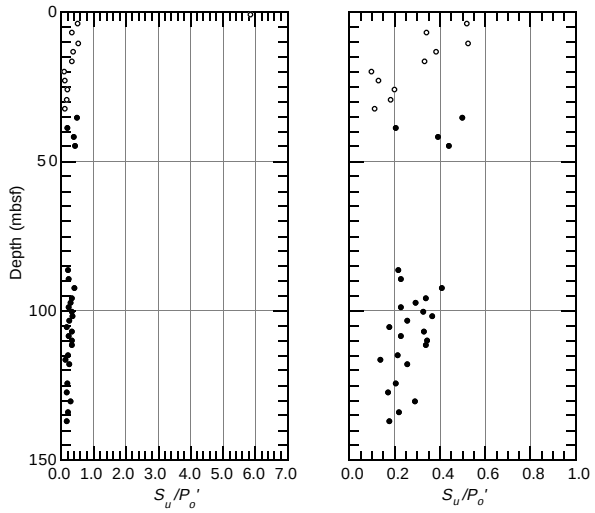

Figure 25. S_u/P_0' for Hole 1053A at two scales. The S_u/P_0' are calculated from bulk density and undrained shear strength data (see "Physical Properties" section [this chapter] for further details). The right-hand panel shows the data on an expanded S_u/P_0' scale.

Table 26. Discrete measurements of resistivity for Hole 1053A.

Core, section, interval (cm)	Depth (mbsf)	Longitudinal resistivity (Ωm)	Transverse resistivity (Ωm)
171B-1053A-			
1H-1, 82.5-85.5	0.83	0.435	0.432
1H-3, 82.5-85.5	3.83	0.460	0.434
1H-5, 82.5-85.5	6.83	0.588	0.588
2H-1, 82.5-85.5	10.33	0.482	0.458
2H-3, 56.5-59.5	13.07	0.519	0.503
2H-5, 84.5-87.5	16.35	0.507	0.487
3H-1, 70-73	19.70	0.505	0.474
3H-3, 80.5-83.5	22.81	0.603	0.531
3H-5, 72-75	25.72	0.552	0.555
4H-1, 78.5-81.5	29.29	0.603	0.613
4H-3, 78-81	32.28	0.590	0.587
4H-5, 78.5-81.5	35.29	0.576	0.526
5H-1, 78.5-81.5	38.79	0.528	0.517
5H-3, 71-74	41.71	0.672	0.626
5H-5, 65.5-68.5	44.66	0.676	0.661
10H-1, 81.5-84.5	86.32	0.556	0.539
10H-3, 81.5-84.5	89.32	0.620	0.595
10H-5, 81.5-84.5	92.32	0.656	0.633
11H-1, 78.5-81.5	95.79	0.678	0.657
11H-3, 55.5-58.5	98.56	0.654	0.650
11H-5, 80.5-83.5	101.81	0.678	0.686
12H-1, 96.5-99.5	105.47	0.597	0.585
12H-3, 81.5-84.5	108.32	0.674	0.628
12H-5, 81.5-84.5	111.32	0.683	0.681
13H-1, 83.5-86.5	114.84	0.627	0.601
13H-3, 81.5-84.5	117.82	0.670	0.625
13H-5, 81.5-84.5	120.82	0.673	0.644
14H-1, 81.5-84.5	124.32	0.690	0.649
14H-3, 81.5-84.5	127.32	0.725	0.738
14H-5, 81.5-84.5	130.32	0.763	0.775
15H-1, 81.5-84.5	133.82	0.727	0.699
15H-3, 81.5-84.5	136.82	0.753	0.727

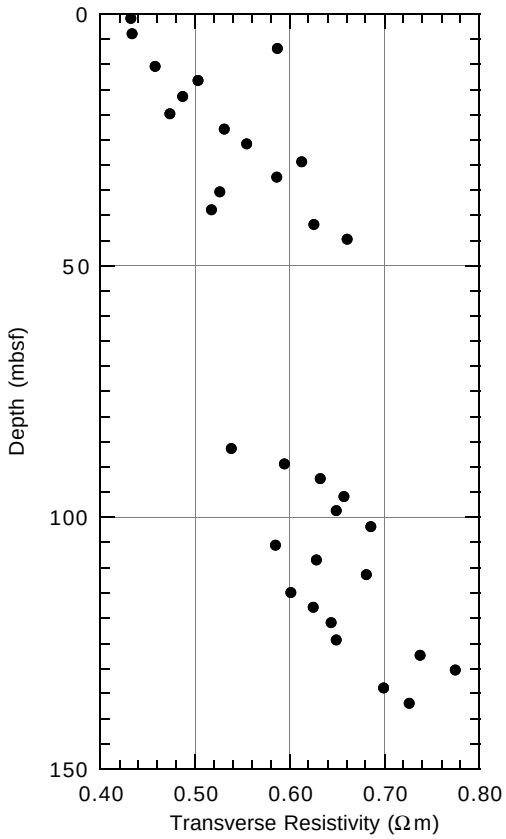

Figure 26. Sediment resistivity for Hole 1053A. Note that transverse resistivity measurements are considered more reliable than longitudinal measurements, because planar unloading cracks that are perpendicular to the core axis bias longitudinal resistivity measurements to higher values.

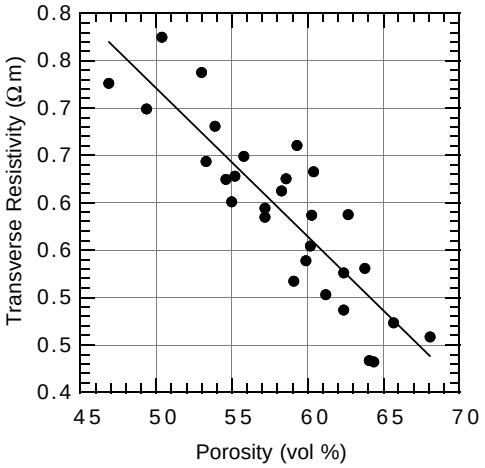

Figure 27. Comparison of transverse resistivity and sediment porosity for Hole 1053A. The line is a linear regression through the data with a slope of 1.50 (r^2 = 0.77).

Table 27. Discrete measurements of thermal conductivity for Hole 1053B.

Core, section, interval (cm)	Depth (mbsf)	Thermal conductivity (W/[m·K])
171B-1053B-		
1H-1, 70-70	0.70	1.15
2H-1, 70-70	4.60	1.17
2H-3, 65-65	7.55	1.06
2H-5, 70-70	10.60	1.14
3H-1, 70-70	14.10	1.12
3H-3, 70-70	17.10	0.53
3H-5, 70-70	20.10	0.34
4H-1, 70-70	23.60	1.12
4H-3, 70-70	26.60	1.10
4H-5, 70-70	29.60	1.17
5H-1, 70-70	33.10	1.16
5H-3, 70-70	36.10	1.16
5H-5, 70-70	39.10	1.22
6H-1, 70-70	42.60	1.17
6H-3, 70-70	45.60	0.65
6H-5, 70-70	48.60	1.19
7H-1, 70-70	52.10	0.74
7H-3, 70-70	55.10	1.15
7H-5, 70-70	58.10	1.21
8H-1, 70-70	61.60	1.17
8H-3, 70-70	64.60	1.19
8H-5, 70-70	67.60	1.19
9H-1, 70-70	71.10	0.80
9H-3, 70-70	74.10	1.15
9H-5, 70-70	77.10	1.35
10H-1, 100-100	80.90	1.18
10H-3, 70-70	83.60	1.18
10H-5, 60-60	86.50	1.25
11H-1, 70-70	90.10	1.13
11H-3, 70-70	93.10	1.24
11H-5, 70-70	96.10	1.30
12H-1, 70-70	99.60	1.21
12H-3, 70-70	102.60	1.25
12H-5, 70-70	105.60	1.32
13H-1, 70-70	109.10	1.24
13H-3, 70-70	112.10	0.74
13H-5, 70-70	115.10	1.25
14H-1, 70-70	118.60	1.28
14H-3, 70-70	121.60	1.31
14H-5, 70-70	124.60	1.30

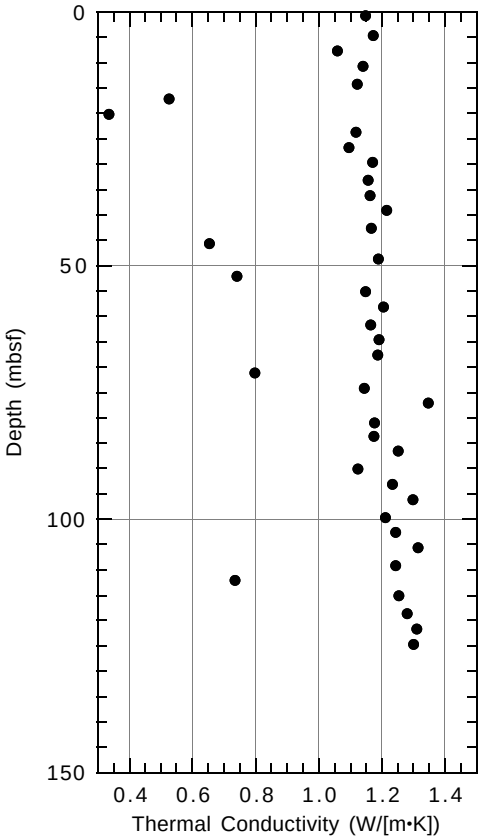

Figure 28. Thermal conductivity for Hole 1053B.

Table 28. In situ Adara temperature tool measurements in Hole 1053B.

Depth (mbsf)	Bottom water temperature (°C)	Sediment temperature (°C)
0	3.965	
22.9		4.174
51.4		4.920
79.9		5.171

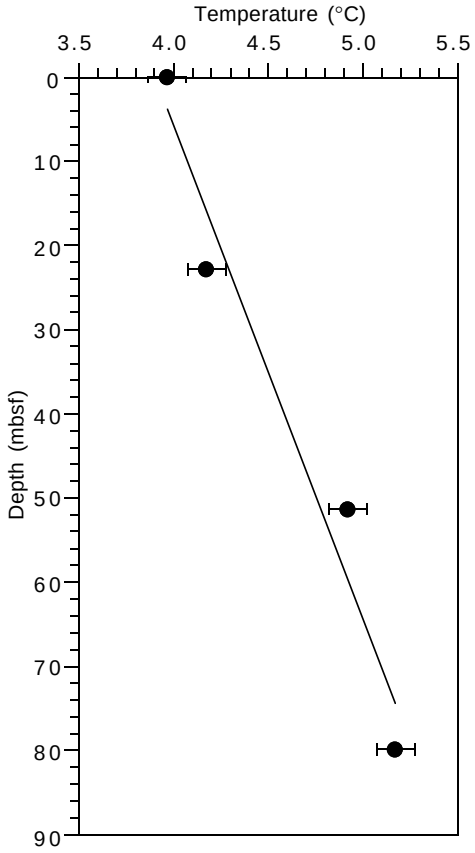

Figure 29. In situ temperature for Hole 1053B. Solid line is a linear fit to the data and has a slope of 17.1°C/km. Error bars show the nominal accuracy associated with the Adara temperature measurements (±0.1°C).

Prior Chapter Contents Next Chapter